Thesis for the degree of Doctor of Philosophy

# Quantum and classical metrology for noise radar

Robert S. Jonsson

Department of Microtechnology and Nanoscience (MC2)
Chalmers University of Technology
Göteborg, Sweden 2024

**Quantum and classical metrology for noise radar**
Robert S. Jonsson
ISBN 978-91-8103-093-8

Acknowledgements, dedications, and similar personal statements in this thesis reflect the author's own views.



Doktorsavhandlingar vid Chalmers tekniska högskola
Ny serie nr 5551
ISSN 0346-718X

Chalmers University of Technology
Department of Microtechnology and Nanoscience (MC2)
SE-412 96 Göteborg, Sweden
Phone: +46 (0)31–772 1000

Printed by Chalmers Digitaltryck
Göteborg, Sweden 2024

**Quantum and classical metrology for noise radar**

Robert S. Jonsson

Applied Quantum Physics Laboratory
Department of Microtechnology and Nanoscience (MC2)
Chalmers University of Technology

# Abstract

We are in an era of rapid advancements in quantum technology, exploring the potential of exploiting quantum phenomena for technological solutions across a wide range of applications. Quantum technologies show promise in areas such as computing, optimisation, communication, sensing, and more. Among these emerging quantum technologies, sensing has perhaps reached the highest level of maturity, with practical applications already available. Quantum radar, a concept from quantum sensing, has garnered significant attention within the radar community, due to the potential of enhancing detection sensitivity compared to classical radar.

This thesis and the appended papers explore measurement protocols for radar-like scenarios. The research spans across two areas, from the classical world to the quantum domain. On the quantum side, the viability and practicality of quantum-enhanced radar is investigated, shedding light on the origin of its potential advantages and the challenges of its realisation. Furthermore, using the tools of quantum metrology, optimal probes for radar-like parameter estimation tasks are established. On the classical side, the development and implementation of an experimental bistatic noise radar system is detailed in terms of a series of signal processing methods.

**Keywords**: Noise Radar, Quantum Radar, Clutter suppression, Model-based Signal Processing, Quantum Metrology, Quantum Fisher Information

*Time is a measure of space,*
*just as a range-finder is*
*a measure of space,*
*but measuring locks us into*
*the place we measure.*

---

Frank Herbert, *Children of Dune*

# List of publications

This thesis is based on the work contained in the following papers, referred to by Roman numerals in the text:

## Noise radar

[I] M. Ankel, **R. Jonsson**, T. Bryllert, L.M.H. Ulander, P. Delsing, "Bistatic noise radar: Demonstration of correlation noise suppression", *IET Radar, Sonar & Navig.* **17**, 3, pp. 351 – 361 (2023).
DOI: `10.1049/rsn2.12345`

[II] M. Ankel, **R.S. Jonsson**, M. Tholén, T. Bryllert, L.M.H. Ulander, P. Delsing, "Experimental Evaluation of Moving Target Compensation in High Time-Bandwidth Noise Radar", *Proceedings of the 20th European Radar Conference*, pp. 1 – 4 (2023).
DOI: `10.23919/EuRAD58043.2023.10289425`

[III] **R.S. Jonsson**, M. Ankel, M. Tholén, T. Bryllert, L.M.H. Ulander, P. Dammert, P. Delsing, "Experimental Analysis of a Clutter Suppression Algorithm for High Time-Bandwidth Noise Radar", *2023 IEEE International Radar Conference (RADAR)*, pp. 1 – 6 (2023).
DOI: `10.1109/RADAR54928.2023.10371039`

[IV] M. Ankel, **R.S. Jonsson**, M. Tholén, T. Bryllert, L.M.H. Ulander, P. Delsing, "Real-Time Bistatic Noise Radar with Adaptive Beamforming", *Accepted for publication at IEEE Radar International Conference 2024, Rennes, France*

## Quantum metrology

[V] **R. Jonsson**, R. Di Candia, M. Ankel, A. Ström, G. Johansson, "A comparison between quantum and classical noise radar sources", *2020 IEEE Radar Conference (RadarConf2020)*, pp. 1 – 6 (2020).
DOI: `10.1109/RadarConf2043947.2020.9266597`

[VI] **R. Jonsson**, M. Ankel, "Quantum Radar – What is it good for?", *2021 IEEE Radar Conference (RadarConf2021)*, pp. 1 – 6 (2021).
DOI: `10.1109/RadarConf2147009.2021.9455162`

[VII] **R. Jonsson**, R. Di Candia, "Gaussian quantum estimation of the loss parameter in a thermal environment", *J. Phys. A: Math. Theor.* **55**, 385301 (2022).
DOI: `10.1088/1751-8121/ac83fa`

[VIII] **R.S. Jonsson**, G. Johansson, "Applications of tri-squeezed states for quantum sensing of two-photon absorption", *Draft manuscript in preparation*

## Publications not included in this thesis

[A] D. Fitzek, **R.S. Jonsson**, W. Dobrautz, C. Schäfer, "Optimizing Variational Quantum Algorithms with qBang: Efficiently Interweaving Metric and Momentum to Tackle Flat Energy Landscapes", *Quantum* **8**, 1313 (2023).
DOI: 10.22331/q-2024-04-09-1313

# Contents

# Acknowledgement

There have been many individuals involved in the work that lead to this thesis and I expect that any attempt at an exhaustive list will be found lacking. I must thank my supervisor Göran Johansson and my co-supervisor Anders Ström for supporting me through these years, for initiating the project, and for believing in me. A gigantic thank you goes out to my collaborator Martin Ankel whose dedication and no-nonsense attitude is a constant reminder that anything is possible if you set your mind to it. I would have never gotten a hold of the field of quantum metrology without Roberto Di Candia. It has been a pleasure to work in the office of the Applied Quantum Physics Laboratory at MC2, Chalmers. A lot of people have come and gone since I started and everyone has contributed to an open and welcoming research environment. In particular, I must thank my office mate Oliver Hahn. Your insightful humour, wide and detailed knowledge as well as excellent taste in culture has brought joy to my time at Chalmers. I also have the great pleasure to be part of the extremely competent Future Technologies group at Saab and I value the many discussions we have had and hopefully will continue to have in the future.

Finally, I thank Caroline for supporting me through this endeavour. Your love keeps me going.

Robert Sven Jonsson, Göteborg, August 2024

# Nomenclature

## Abbreviations & Acronyms

| | |
|---|---|
| **ADC** | Analogue-to-Digital Converter |
| **CCN** | Classically Correlated Noise |
| **CFAR** | Constant False Alarm Rate |
| **FI** | (Classical) Fisher Information |
| **CNF** | Correlation Noise Floor |
| **CPI** | Coherent Processing Interval |
| **CRLB** | Cramér-Rao Lower Bound |
| **ECA** | Extensive Cancellation Algorithm |
| **FFT** | Fast Fourier Transform |
| **GLRT** | Generalised Likelihood Ratio Test |
| **INR** | Interference-to-Noise Ratio |
| **LRT** | Likelihood Ratio Test |
| **PDF** | Probability Density Function |
| **PRI** | Pulse Repetition Interval |
| **QI** | Quantum Illumination |
| **QFI** | Quantum Fisher Information |
| **Radar** | Radio Detection and Ranging |
| **RF** | Radio Frequency |
| **ROC** | Receiver Operating Characteristic |
| **SLD** | Symmetric Logarithmic Derivative |
| **SNR** | Signal-to-Noise Ratio |
| **TMSV** | Two-Mode Squeezed Vacuum |
| **UAV** | Uncrewed Aerial Vehicle |
| **ULA** | Uniform Linear Array |
| **WACQT** | Wallenberg Centre for Quantum Technology |

## Notation, Symbols & Operations

| | |
|---|---|
| $x, X$ | Cursive: Scalar quantity |
| $\mathbf{x}$ | Lower-case boldface: Vector quantity |
| $\mathbf{X}$ | Upper-case boldface: Matrix quantity |
| $\vec{X}$ | Arrow: Vector field |
| $\hat{x}, \hat{X}$ | Hat: Quantum mechanical operator |
| $\lvert x\rangle$ | Pure quantum state |
| $\rho$ | Density operator / Mixed quantum state |
| $\mathbf{X}^\top$ | Transpose of $\mathbf{X}$ |
| $\mathbf{X}^\dagger$ | Conjugate (Hermitian) transpose of $\mathbf{X}$ |
| $\mathbf{X}^*$ | Complex conjugate |
| $\mathbf{X}^{-1}$ | Inverse of invertible matrix $\mathbf{X}$ |
| $\mathbf{X}^+$ | Moore-Penrose pseudo-inverse of $\mathbf{X}$ |
| $\mathbf{P}_\mathbf{X}$ | Projection matrix onto the column space of $\mathbf{X}$ |
| $\otimes$ | Kronecker / Tensor product |
| $\odot$ | Hadamard / Elementwise product |
| $\mathcal{F}_\downarrow[\cdot]$ | Column-wise discrete Fourier transform |
| $\mathcal{F}_\rightarrow[\cdot]$ | Row-wise discrete Fourier transform |
| $\mathrm{i} = \sqrt{-1}$ | The imaginary unit |
| $\mathfrak{Re}[\cdot], \mathfrak{Im}[\cdot]$ | Real and imaginary part: $z = \mathfrak{Re}[z] + \mathrm{i}\mathfrak{Im}[z]$ |
| $\mathcal{CN}(\boldsymbol{\mu}, \boldsymbol{\Sigma})$ | Complex normal distribution with mean $\boldsymbol{\mu}$ and covariance matrix $\boldsymbol{\Sigma}$ |
| $\mathbb{E}[\cdot]$ | Expectation value over classical distribution |
| $\mathrm{var}[\cdot]$ | Variance: $\mathrm{var}[X] = \mathbb{E}[X^2] - (\mathbb{E}[X])^2$ |
| $\langle\hat{O}\rangle$ | Expectation value of quantum state |
| $\mathrm{tr}[\cdot]$ | Trace |
| $\det[\cdot]$ | Determinant |
| $\mathbb{I}, \mathbb{I}_N$ | Identity matrix. Subscript denotes dimension $N \times N$ if needed in context. |
| $[\mathbf{X}]_{i,j}$ | The element on row $i$ and column $j$ of matrix $\mathbf{X}$. |
| $[\mathbf{X}\ \mathbf{Y}]$ | Concatenation of matrices where the columns of $\mathbf{Y}$ are added to the right of the columns of $\mathbf{X}$. |

Chapter 1

# Introduction

## 1.1 Background

The basic principle of radar was demonstrated already in 1904 by Christian Hülsmeyer when he used his invention of the *Telemobiloskop* to detect passing ships on the river Rhine [1, 2]. Today, radars are a relatively common technology, with applications not only within the military disciplines, but also for civil sectors, such as air traffic surveillance, navigation and weather forecasting. A radar system operates by transmitting electromagnectic waves into the environment and 'listening' for echoes generated by the reflection off of objects, referred to as *targets*. In fact, RADAR is an acronym for RAdio Detection and Ranging describing the use of radio waves to detect and estimate properties of targets. For the modern practical radar applications of today, a classical (as in non-quantum) description of electromagnetics is usually sufficient to understand the underlying physics, because the relevant energies vastly overwhelm the scale of individual photons. However, inspired by the potential benefits in harnessing underlying quantum phenomena, there have been research efforts towards developing quantum radars.

Today, we understand not only how quantum systems behave, but also their metrological properties [3]. By metrology, we mean the theory, or the science, of measurement which can be understood as follows. In a quantitative experiment the experimentalist uses calibrated equipment to measure some quantity of interest. Fundamentally, such an experiment must respect the uncertainties mandated by quantum mechanics. In many real-life applications, noise and other errors overwhelm the quantum mechanical uncertainties. However, there are situations where careful analysis and understanding of quantum mechanics allows us to do better than any purely classical probe. These concepts may be collectively referred to as quantum enhanced sensing and the theory of this analysis is that of metrology [4]. As an example, the LIGO gravitational wave detector uses a quantum enhanced

protocol to push the sensitivity beyond the standard limits of precision [5, 6].

## 1.2 Noise radar

Many conventional radar systems, such as air surveillance radars, operate by transmitting sequences of pulses. Between the pulses, the radar switches to receiver mode and records possible electromagnetic reflections off of objects in the environment. By estimating time-of-flight, the distance of targets can be determined. Noise radar is an alternative to pulsed operation, instead using a continuous transmission with a non-repeating signal that may be indistinguishable from thermal noise. The idea to use noise radar is not new [7], but the technology has not existed for it to be realised as practical and useful systems. There have been experimental demonstrators, such as the system used in Refs. [8, 9], but, as far as we know, no commercially available noise radar.

In a noise radar, the measurement of target signals is performed by correlating the received signal with a retained reference of the transmitted signal. This introduces several challenges compared to pulsed operation [10]. One may justify dealing with those challenges for several reasons. For one, a noisy waveform enables processing that is unambiguous in both range and velocity. By processing a large time-bandwidth product, the instantaneous power spectral density can be kept low, possibly reducing the risk that the radar signal is intercepted [11–13]. There have been investigations into using noise radar for applications such as ground penetrating and through-the-wall sensing [14–16] as well as imaging with short-range synthetic aperture radar [17]. Passive radar, using existing transmitters of opportunity instead of a cooperating transmitter, faces similar challenges with the use of waveforms that typically are noisy, such as issues caused by correlation processing [18–20].

## 1.3 Quantum Radar

Going by the patent of Ref. [21], a quantum radar is a radar system that circumvents the Rayleigh diffraction limit by using "*a signal including a plurality of entangled particles*" for the purpose of resolving targets better than a classical system. We must acknowledge that the term can refer to different things depending on the context [22–24]. From the description found in literature, there is some ambiguity as to whether it refers to a theoretical protocol or a physical device. The device described in the patent of Ref. [25] uses a pair of entangled signals to realise a quantum advantage over a classical benchmark with the protocol of Quantum Illumination (QI). The aforementioned QI protocol was named so in Ref. [26], where, building on the work of Sacchi [27, 28], an entangled signal-idler pair was shown able to significantly outperform single-photon signals in the task of deciding whether a weakly reflecting target is present in a noisy background – a scenario that certainly has radar-like quailities. Further analysis proved that this

advantage could overtaken by a weak coherent state probe [29]. However, Tan *et al.* showed in Ref. [30] that Gaussian state QI can achieve an entanglement advantage of a factor of 4 in the effective SNR, commonly referred to as "the 6 dB advantage". The QI protocol is particularly interesting from a purely theoretical point of view because of the peculiar feature that a quantum advantage is achieved over the classical benchmark even though the initial entanglement does not survive the process. It thus calls into question what role entanglement has as a metrological resource. However, this question is beyond the scope of this thesis. It is important to note that, although QI performs the detection part of radar operation, it requires prior knowledge of the transmit-to-receive path length to realise the advantage. That is, the protocol is not able to perform detections at an unknown distance. Nevertheless, the QI protocol has been understood as a type of quantum radar [22]. There are other protocols claiming to be quantum radars, where estimation of time-of-flight is incorporated [31].

A metrological protocol such as QI describes not only the probe state and measurement scenario, but also the receiver setup that measures the optimal observable. For the QI protocol, receiver structures based on Optical Parametric Amplification (OPA) and Phase-Conjugation (PC), respectively, were described by Guha and Erkmen [32] which lead to the patent of Ref. [25]. These receivers are *sub*-optimal because they realise only a factor of 2 advantage. A theoretical receiver structure based on iteration of sum-frequency generation has been shown to realise the full advantage [33], but experimental realisation of that concept is not feasible.

A no-go result shown by Nair [34]. It says that no quantum advantage can be achieved over a coherent state if the discrimination is done against a vacuum background. A consequence of this no-go result is that the discrimination must be against a noisy background. At ambient room temperature conditions the visible light spectrum does not satisfy this requirement. On the other hand, noise is naturally present at room temperature in the microwave regime (approximately 300 MHz to 30 GHz). The necessary technology, such as number resolving microwave photon detectors, is not yet developed. This technology gap was approached in Ref. [35], with the proposed solution of using an opto-mechanical interface to coherently convert photons between visual light frequencies and microwaves. This scheme allows for the generation and detection of entangled photons to be done at optical frequencies, where the necessary technology is available, while the probing is done with microwaves, where the background is noisy and an advantage may be had. Around this point in time general media started to write about quantum radar applications and realisations, see, *e.g.*, Refs. [36, 37]. These reports, targeting a non-expert audience, tended towards creative interpretations of the quantum properties, such as the role of quantum entanglement, and overstated the maturity of the technology. For example, the dubious statement that a quantum radar can detect stealth aircraft was picked up as a revolutionary technological achievement [36]. Nevertheless, reports like these increased awareness of the ideas and likely influenced decisions leading to further research funding.

On the academic side, there have been several publications claiming experimental demonstration of the QI protocol, *e.g.*, Ref. [38]. These results have been challenged as to whether they fully realised the QI protocol [39] on the grounds that coincidence-counting setups do not fully exploit the initial entanglement. In 2015, the QI protocol was demonstrated with a sub-optimal OPA receiver [40]. Another experimental demonstration was performed by England *et al.* [41]. They used optics and coincidence counting and a jamming laser was used to artificially add background photons to the detector. Similarly, Blakely *et al.* [42] presented results of performing a similar QI-like task for LIDAR[1] applications.

A variation on the QI protocol was put forward in Refs. [43, 44] with experimental results in the microwave regime with free-space propagation, showing how entangled signals outperform correlated thermal noise signals. These results garnered some attention because the experiments showed a quantum advantage with a simple heterodyne detection scheme. The demonstrated protocols were described as a type of quantum *noise* radar. While the initial pre-print of Ref. [45], published as `arXiv:1908.03058` in 2019, presented similar results at that point in time, the final published version clarifies that ideal photon number detection is required to realise the advantage. The pre-print result was also reported as a quantum radar [46]. Criticism as to the correctness of these results in the microwave regime as implementations of QI were raised by Shapiro in Ref. [39], where one of the main arguments is that the correlated thermal noise used as a classical reference system is not optimal and that, with minor modifications, the classical reference system would perform equivalently to the quantum enhanced system. More microwave quantum illumination demonstrations have been reported, using measurement techniques that could realise a sub-optimal quantum advantage [47, 48] Other, theoretical receiver structures have also been suggested, such as Ref. [49]. It has been shown that it is possible to utilise a transformation from signal-idler correlations to idler displacement [50, 51] to realise a receiver, which may be possible to implement as a sequential protocol [52]. Improvements in the enabling microwave quantum technology are also being made, with demonstrations of microwave single-photon detection [53, 54].

There are protocols other than QI that seek to exploit quantum properties in radar-like tasks [55], such as improving the measurement accuracy of distance with pulse compression [56] and velocity by utilising the Doppler shift [57]. Additionally, there have been extensions to the target model, such as a target cloaking by phase-shifting the illuminating radiation [58] or a target signal that fluctuates over the observation interval [59]. There have also been some investigations into QI with three-mode entangled Gaussian states [60]. To this day, interest in quantum illumination for radar continues [61, 62].

Overall, the prospects of real-life application of these quantum radars lean towards close-range probing, such as a non-invasive scanning of sensitive samples, rather

[1] LIDAR: LIght Detection And Ranging

than competing with conventional radars that can find targets at distances of up to hundreds of kilometres.

## 1.4 Thesis project and overview

This thesis is the outcome of a research project jointly undertaken by Saab Ab and Chalmers University of Technology within the Wallenberg Centre for Quantum Technology (WACQT) programme. The project started out in the field of quantum radar, with a plan to develop the theory and perform experiments in the microwave regime. At the time (the year 2019), there were recent publications with experimental results that indicated that quantum illumination and similar protocols may be applicable for real-world radar systems, and the initial direction of the research project was to understand and, if possible, replicate and improve on these results. The project was to be executed by two PhD students, Martin Ankel and the author of this thesis, with responsibilities split between theory and experimental work. This thesis covers the theory side of the project. Along the way, the experimental part of the project instead ended up in the development of a non-quantum, experimental noise radar. This lead to a two-way split in the theory research topics with one part focusing on signal processing for noise radar and the other part expanding the analysis of quantum radar to adjacent metrology topics. The theoretical material in this thesis is organised according to a (hopefully) coherent progression rather than following the chronology of the project.

The rest of the thesis is organised as follows. The next two chapters present and develop the theory that is used in the results of the appended papers. Chapter 2 develops a noise radar system model, where the signals involved are derived from transmission to target detection. The material in Chapter 2 roughly follows the chronology of the publication history of the appended **Papers I-IV**. Focus is given to challenges in processing non-periodic, noisy waveforms. Chapter 3 moves on to quantum mechanics and metrological aspects as a foundation for **Papers V-VIII**. A detailed description of quantum illumination is presented in a formulation that should be accessible to a reader familiar with conventional radar. Next, Chapter 4 gives a short summary of each of the appended papers. Finally, Chapter 5 reflects on the project and results.

Overall, the text in this thesis strives to maintain a consistent notation through all chapters. It is unavoidable that some variables are being repurposed between chapters, but all expressions should be unambiguous in context. A consequence is that the expressions in the main text sometimes differ from those in the appended papers in terms of variables, sign convention etc. For the entire thesis, vectors are denoted by lowercase boldface font, *e.g.*, $\mathbf{x}$, while matrices use uppercase boldface font, *e.g.*, $\mathbf{X}$. All vectors are organised as column vectors and, when they appear, row vectors are always written as the transpose ($\top$) or conjugate transpose ($\dagger$) of a column vector.

Chapter 2

# Noise Radar

## 2.1 Radar fundamentals

A radar system operates by the transmission and reception of electromagnetic waves. Since electromagnetic waves may scatter off of objects, reflected signals can be detected by the radar at reception. The radar system extracts target information (distance, velocity, etc.) from these received signals and reports them to an operator. To design a processing algorithm that performs this task, it is necessary to understand what happens to the signal at each step from transmission to detection. This chapter presents how the signals are modelled in the noise radar, followed by a presentation of some details regarding signal processing. Here, we are concerned with a simplified statistical model, and details regarding hardware such as amplifiers, filters etc. are omitted. We present the theory for quasi-monostatic setups, where the radar transmitter and receiver are considered separate systems, but located at the same site. The appended research papers on noise radar contains such experimental setups, but also true bistatic separation, where the transmitter and receiver system are located far from each other. Bistatic separation introduces many technical challenges, such as time and frequency synchronisation, positioning, etc. However, from a mathematical point of view, most of the theory is equivalent for monostatic and bistatic setups. When modelling target signals, we will assume that the relevant scattering happens in the electromagnetic far-field. While it will not be of central importance to this text, this means that, for a monostatic radar, the return power $P_R$ of a point target at a distance $R$ can be related to the transmitted power $P_T$ as

$$P_R \propto \frac{P_T}{R^4}, \tag{2.1}$$

equivalently to the standard radar range equation derivation found in textbooks, *e.g.*, Refs. [63, 64].

This chapter is organised as follows. First, we model strictly temporal signals, with a noise radar able to measure distance and radial velocity. In the temporal domain, the noise radar correlation processing is discussed and, in this context, the issue of multiple target signals and the correlation noise floor are introduced. Next, a detector function for noise radar is derived and some algorithmic approaches to handle the correlation noise floor are presented. Finally, we expand the model to handle spatial information and discuss the suppression of unwanted signals from certain directions in Section 2.6.

## 2.2 Temporal Signal modelling

The noise radar waveform is generated from a noisy reference $\mathbf{x}_0 \sim \mathcal{CN}(\mathbf{0}, \mathbb{I}_M)$ consisting of $M$ complex Gaussian pseudo-random samples. The radar will transmit a continuous signal $x(t)$ generated by the sequence $\mathbf{x}$, which is the original random sequence $\mathbf{x}_0$ matched to the system bandwidth. We write the discrete signals, sampled at rate of $f_s$, as

$$x_m = x(m/f_s), \quad m = 0, 1, \ldots, M-1 \tag{2.2}$$

and collect sequences in a vector as

$$\mathbf{x} = [x_0, x_1, \ldots, x_{M-1}]^\top . \tag{2.3}$$

The processing will be applied to sequences of length $M$, which is arbitrary, but large. We interchangeably refer to the data and its length as the coherent processing interval (CPI). The discrete representation of the transmitted signal $\mathbf{x}$ can be reconstructed digitally by knowledge of the pseudo-random seed and system characteristics. The radar operates at a carrier frequency $f_c$ in the microwave regime, which keeps components reasonably small. We will assume that the bandwidth of the transmitted signal $x(t)$ may be significant, but not larger than approximately 20% relative $f_c$, such that separation of carrier and base-band makes sense. Since we are mainly concerned with noise radar, we will have to accommodate our models for continuous transmission and long integration times.

### 2.2.1 Target signal

The transmit-to-receive channel for one target is modelled as follows and as illustrated in Figure 2.1. First, the noisy reference signal is up-converted to the carrier frequency as

$$x_{\mathrm{RF}}(t) = x(t) \exp\left[2\pi \mathrm{i} f_c t\right] . \tag{2.4}$$

The signal $x_{\mathrm{RF}}(t)$ is transmitted and assumed to scatter off of a target in the environment. After a delay $\tau(t)$, the reflected signal arrives at the radar receiver as

$$\begin{aligned} y_{\mathrm{RF}}(t) &= \theta(t) x_{\mathrm{RF}}\left[t - \tau(t)\right] \\ &= \theta(t) x\left[t - \tau(t)\right] \exp\left[2\pi \mathrm{i} f_c (t - \tau(t))\right] , \end{aligned} \tag{2.5}$$

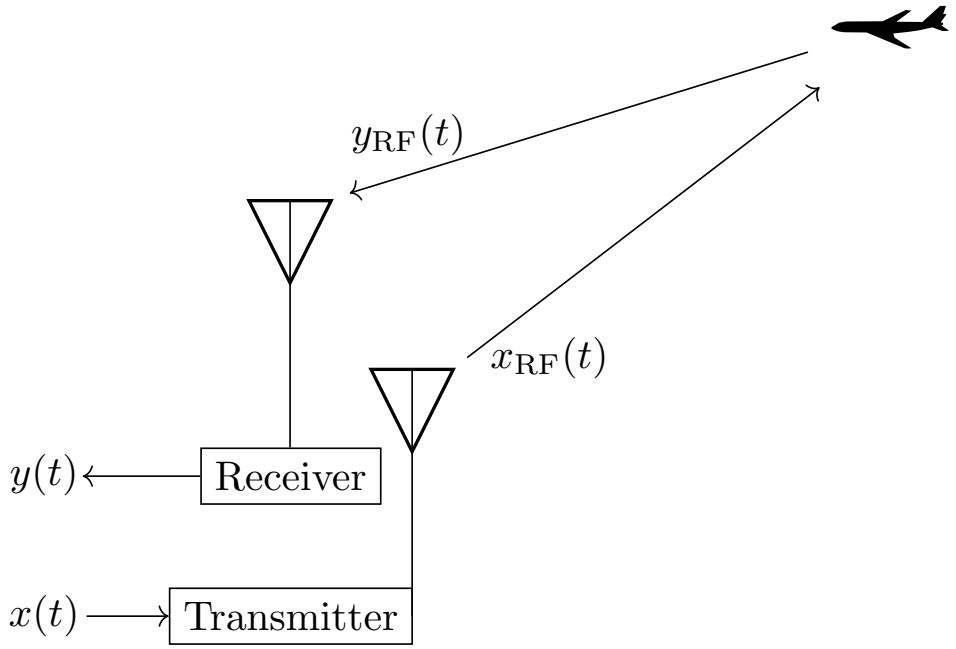


**Figure 2.1:** Schematic overview of the transmit-to-receive channel. The reference signal $x(t)$ is up-converted to $x_{\mathrm{RF}}(t)$ and transmitted. After a travel time of $\tau(t)/2$, the transmitted signal scatters off of a target. Finally, after another travel time of $\tau(t)/2$, the receiver captures the scattered signal $y_{\mathrm{RF}}(t)$ and down-converts it to $y(t)$.

where $\theta(t)$ is the target scattering function. Finally, the receiver down-converts the signal back to baseband as

$$\begin{aligned} y(t) &= y_{\mathrm{RF}}(t) \exp\left[-2\pi \mathrm{i} f_c t\right] \\ &= \theta(t) x\left[t - \tau(t)\right] \exp\left[-2\pi \mathrm{i} f_c \tau(t)\right]. \end{aligned} \tag{2.6}$$

We will refer to the baseband signal $y(t)$ and its discrete representation $\mathbf{y}$ interchangeably as the received signal or the observed signal.

We must specify the time-dependent delay function $\tau(t)$ which expresses how much the signal is delayed with respect to the time of transmission when it arrives at the receiver. The derivation follows closely Ref. [65] where the expression is derived in the radar system frame, and holds for targets moving at non-relativistic speeds. Determining the delay time is central for the radar to be able to detect the distance to the target. In the model of the delay time, as presented below, the resulting expression also shows how both Doppler modulation and time dilation affect the received signal.

Let $R(t)$ denote the instantaneous distance between the target and the radar system at time $t$, referenced with respect to the time of transmission. Since the signal travels to the target and back again, the signal 'interacts' with the target at time $\tau(t)/2$, at which time the distance to the target is $R\left(t - \frac{\tau(t)}{2}\right)$. The total

transmit-to-receive distance covered by the signal is $c\tau(t)$, where $c$ is the speed of light. Mathematically, we can express this relation between the distance and delay time as

$$\frac{c}{2}\tau(t) = R\left(t - \frac{\tau(t)}{2}\right). \tag{2.7}$$

To solve for the delay, we compute the linear Taylor expansion of $\tau(t)$ around a reference delay time $\tau_0$, as

$$\tau(t) = \tau_0 + \dot{\tau}\left(\tau_0\right)\left(t - \tau_0\right), \tag{2.8}$$

where reference time corresponds to a reference target distance $R_0 = \frac{\tau_0 c}{2}$. Linear evolution of the delay time corresponds to a constant relative velocity. A higher order expansion is needed to model accelerating targets. The function $\dot{\tau}(t)$ is found by taking the time derivative of Eq. (2.7) as

$$\dot{\tau}(t) = \frac{2}{c}\left(1 - \frac{\dot{\tau}(t)}{2}\right)\dot{R}\left(t - \tau(t)/2\right), \tag{2.9}$$

where $\dot{R}(t)$ is the radial velocity of the target at time $t$. Since we are modelling constant velocity over observation interval, we denote it by $v_0 = \dot{R}\left(t\right)$. Solving Eq. (2.9) for $\dot{\tau}(t)$ and evaluating at $t = \tau_0$, we have

$$\dot{\tau}\left(\tau_0\right) = \frac{2v_0}{c + v_0}. \tag{2.10}$$

Inserting the expression for $\dot{\tau}\left(\tau_0\right)$ in Eq. (2.8) and rearranging yields

$$t - \tau\left(t\right) = st - s\tau_0, \tag{2.11}$$

where we have introduced the *stretch factor*

$$s = \frac{c - v_0}{c + v_0}. \tag{2.12}$$

Due to the relative movement between the target and radar, the stretch factor describes the time dilation of the received signal.

The received RF signal is $\tilde{y}(t) = \theta(t)\tilde{x}\left(st - s\tau_0\right)$, and the corresponding base-band signal is

$$y(t) = \theta'(t)x\left(st - s\tau_0\right)\exp\left[2\pi \mathrm{i} f_c t(s-1)\right], \tag{2.13}$$

where we incorporated a constant phase in the scattering function $\theta'(t) = \theta(t)\mathrm{e}^{-2\pi \mathrm{i} f_c s\tau_0}$. In general, we will consider $\theta'(t)$ to be unknown, so the addition of a constant phase will be irrelevant within the model. Formally, when considering time stretching we require that the total energy of $x(t)$ is conserved, which introduces a stretch dependent scaling factor. For our purposes, this scaling is also incorporated in the unknown scattering function $\theta'(t)$.

In practically all radar applications, the radial velocity is minuscule with respect to the speed of light and we can take $\frac{|v_0|}{c} \ll 1$, such that $s = 1 - 2\frac{v_0}{c} + \mathcal{O}\left(\frac{v_0^2}{c^2}\right)$. Then, the received baseband signal can be modelled

$$y(t) = \theta'(t)x\left[\left(1 - \frac{2v_0}{c}\right)\left(t - \frac{2R_0}{c}\right)\right]\exp\left[-2\pi \mathrm{i} f_c t \frac{2v_0}{c}\right]. \tag{2.14}$$

Here, the factor $\exp\left[-2\pi \mathrm{i} f_c t \frac{2v_0}{c}\right]$ produces the "normal" Doppler modulation which is more readily expressed in terms of the wavelength $\lambda = \frac{c}{f_c}$. It is common in conventional radar, with Doppler tolerant waveforms, to drop the $2\frac{v_0}{c}$-term in the base-band waveform and consider only Doppler processing. However, for fast targets and processing with large time-bandwidth products, the mismatch loss with a noisy waveform may be significant if one does not compensate for time dilation in the baseband.

Since treatment presented here is restricted to the monostatic radar setup and considers only target moving with constant radial velocity, there are some obvious extensions. In Ref. [65], the authors also compute a second order Taylor expansion in Eq. (2.8) to model targets with constant acceleration. Even targets moving with constant velocity with respect to the ground will exhibit some amount of acceleration with respect to the radar system. In the bistatic setup, the derivation follows equivalent steps as presented here, but the transmit and receive channels have to be treated separately, and the resulting stretch factor involves more parameters, see *e.g.*, Refs. [66, 67] for details.

The noise radar system samples the received signal at a rate $f_s$ and implements digital processing. At time $t_m = \frac{m}{f_s}$, the observed signal sampled from Eq. (2.14) is then

$$\begin{aligned} y_m &= y\left(t_m\right) \\ &= \theta'\left(\frac{m}{f_s}\right) x\left[\left(1 - \frac{2v_0}{c}\right)\left(\frac{m}{f_s} - \frac{2R_0}{c}\right)\right]\exp\left[-2\pi \mathrm{i} m \frac{2v_0}{f_s \lambda}\right] \end{aligned} \tag{2.15}$$

and, again, we collect $M$ samples in a vector $\mathbf{y} = [y_0, y_1, \ldots, y_{M-1}]^\top$. Each sample corresponds to a distance cell of size $\Delta R = \frac{c}{2f_s}$. To simplify the notation, we define the Doppler frequency[1]

$$f_\mathrm{D} = -\frac{2v_0}{\lambda}. \tag{2.16}$$

Now, we assume that the target scattering function is constant over the observation interval,

$$\theta'\left(\frac{m}{f_s}\right) = \theta', \quad \text{for all } m = 0, 1, \ldots, M-1. \tag{2.17}$$

[1]The Doppler sign convention can be understood as follows. An approaching target will have a negative radial velocity, because the distance is reducing. At the same time, the Doppler effect will cause the observed frequency to increase for an approaching target, meaning the Doppler shift will be positive.

This assumption may fail for several reasons. If the target is not perfectly pointlike, electromagnetic scattering may vary significantly as the target moves and is illuminated by the radar from different angles. By introducing the vector $\mathbf{h}(R_0, v_0)$ with elements

$$[\mathbf{h}(R_0, v_0)]_m = x\left[\left(1+\frac{f_\mathrm{D}}{f_c}\right)\left(\frac{m}{f_s}-\frac{2R_0}{c}\right)\right]\exp\left[2\pi \mathrm{i} m\frac{f_\mathrm{D}}{f_s}\right], \tag{2.18}$$

the observed target signal can be expressed

$$\mathbf{y} = \theta'\mathbf{h}(R_0, v_0). \tag{2.19}$$

The assumptions that lead us to Eq. (2.19) will be retained for the rest of this chapter. Unless explicitly stated, we will incorporate all amplitude information in the scalar $\theta'$ and normalise the signal vector, *i.e.*, $||\mathbf{h}(R_0, v_0)||^2 = 1$.

### 2.2.2 Multisignal modelling

In any radar scenarios we can expect to receive reflections from more than one object, and not all of these objects may be targets of interest. We refer to uninteresting signals as *clutter* while any interesting signals are referred to as *targets*. Each individual signal is modelled by Eq. (2.19). For now, only signals from our own system are modelled.

The clutter environment is modelled as $P_C$ independent scattering points with no scattering between them. That is, the observed digital signal is the superposition of the signal from each scattering point, which we write as

$$\begin{aligned}\mathbf{y}_C &= \sum_{p=1}^{P_C}\theta_p\mathbf{h}(R_p, v_p)\\ &= \mathbf{H}_C\boldsymbol{\theta}_C.\end{aligned} \tag{2.20}$$

Here,

$$\mathbf{H}_C = \begin{bmatrix}\mathbf{h}(R_1, v_1) & \mathbf{h}(R_2, v_2) & \dots & \mathbf{h}(R_{P_C}, v_{P_C})\end{bmatrix} \tag{2.21}$$

is an *observation matrix* of size $M \times P_C$, and $\boldsymbol{\theta}_C = \begin{bmatrix}\theta_1 & \theta_2 & \dots & \theta_{P_C}\end{bmatrix}^\top$ is a vector of the complex amplitudes.

## 2.3 Noise radar processing

At the simplest level, noise radar processing involves correlating the observed signal $\mathbf{y}$ with the digital reference $\mathbf{x}$. If a strong correlation is observed, target presence can be declared. However, the analysis is slightly more complicated, since a given target may have almost any possible distance and velocity. Instead, the correlation should be performed between the observed signal and the target signal

model $\mathbf{h}$, which depends on $\mathbf{x}$. This means that, in principle, we want to compute the cross-correlation between $\mathbf{y}$ and a large number of signal vectors $\mathbf{h}$. In this section, we discuss some aspects regarding computation of the 2D cross-correlation

$$[\mathbf{Z}]_{i,j} = \mathbf{h}^{\dagger}\left(R_i, v_j\right)\mathbf{y}. \tag{2.22}$$

for a Range-Velocity grid with range cells $R_i$ and velocity cells $v_j$. For the range cells, the computation of $[\mathbf{Z}]_{i,j} = z_{i,j}$ is performed in the frequency domain, as the correlation for different delays is efficiently implemented with the Fast Fourier Transform (FFT) algorithm. In particular, for zero velocity ($v_0 = 0$) we can compute the vector of correlations as

$$\mathbf{z}_0 = \mathcal{F}_{\downarrow}^{-1}\left[\mathcal{F}_{\downarrow}\left[\mathbf{h}^{*}\left(0,0\right)\right] \odot \mathcal{F}_{\downarrow}\left[\mathbf{y}\right]\right], \tag{2.23}$$

where $\mathbf{h}\left(0,0\right) = \mathbf{x}$, see Eq. (2.18). Here, $\mathcal{F}\left[\cdot\right]$ denotes the (discrete) Fourier transform and the subscript $\downarrow$ denotes that the transform is applied column-wise. After a shift in the indices, the correlation vector has elements corresponding to different range cells, as

$$\mathbf{z}_0 = \begin{bmatrix}\mathbf{h}^{\dagger}\left(0,0\right)\mathbf{y} & \mathbf{h}^{\dagger}\left(\Delta R,0\right)\mathbf{y} & \dots & \mathbf{h}^{\dagger}\left((M-1)\Delta R,0\right)\mathbf{y}\end{bmatrix}^{\top}, \tag{2.24}$$

where $\Delta R = \frac{c}{2f_s}$ is the range cell size. For non-zero velocities, we can compute the correlation with a Doppler shifted signal vector as

$$\mathbf{z}_j = \mathcal{F}_{\downarrow}^{-1}\left[\mathcal{F}_{\downarrow}\left[\mathbf{h}^{*}\left(0,v_j\right)\right] \odot \mathcal{F}_{\downarrow}\left[\mathbf{y}\right]\right], \tag{2.25}$$

which requires the computation of $\mathbf{h}\left(0,v_j\right)$ from $\mathbf{x}$ for each $v_j$. If the velocity grid is large, with many $v_j$, the 2D cross-correlation grid is computationally expensive. To lower computational load, we implement an approximate method, referred to as batch processing. By separating the observed signal into several batches, the velocity information can be extracted by applying a Fourier transform in a manner similar to pulse-Doppler radar.

As before, the received signal $\mathbf{y}$ consists of the $M$ samples which cover the coherent processing interval. In the case of batch processing, both the observed signal and the reference signal are separated into $B$ batches of length $N$. To not introduce unnecessary complications regarding truncation, we take $BN = M$. The signal vectors of each batch are identified by subscript $b = 0, 1, \dots, B-1$, with the elements $\mathbf{x}_b = \begin{bmatrix}x_{bN} & x_{bN+1} & \dots & x_{N(b+1)-1}\end{bmatrix}^{\top}$ and $\mathbf{y}_b = \begin{bmatrix}y_{bN} & y_{bN+1} & \dots & y_{N(b+1)-1}\end{bmatrix}^{\top}$. For each batch, the correlation is computed as

$$\mathbf{c}_b = \mathcal{F}_{\downarrow}^{-1}\left[\mathcal{F}_{\downarrow}\left(\mathbf{x}_b^{*}\right) \odot \mathcal{F}_{\downarrow}\left(\mathbf{y}_b\right)\right], \tag{2.26}$$

and the result from all the batches in the CPI can be represented in the matrix

$$\mathbf{C} = \begin{bmatrix}\mathbf{c}_0 & \mathbf{c}_1 & \dots & \mathbf{c}_{B-1}\end{bmatrix}. \tag{2.27}$$

Each row in $\mathbf{C}$ is separated by the time $1/f_s$, sampling the correlation with a particular distance. Each column of $\mathbf{C}$ is separated by the time $N/f_s$. By convention, the high sample rate of the rows is referred to as 'fast-time' while the lower sample rate of the columns is referred to as 'slow-time'.

Let us assume that the observed signal is noise-free and contains only the signal of one target at distance $i\Delta R$ moving with radial velocity $v$, as $\mathbf{y} = \theta\mathbf{h}\left(i\Delta R, v\right)$. Then, the elements of $\mathbf{C}$ are

$$\begin{aligned}\left[\mathbf{C}\right]_{i,b} &= \mathbf{x}_b^{\dagger}\mathbf{y}_b \\ &= \theta S_b \exp\left[2\pi \mathrm{i} b \frac{N f_\mathrm{D}}{f_s}\right],\end{aligned} \tag{2.28}$$

where the coherent sum over fast-time elements is

$$S_b = \sum_{n=0}^{N-1} x^*\left(t_{n,b}\right) x\left[\left(1+\frac{f_\mathrm{D}}{f_c}\right) t_{n,b}\right] \mathrm{e}^{2\pi \mathrm{i} n \frac{f_\mathrm{D}}{f_s}} \tag{2.29}$$

and where the reference is sampled at the time steps

$$t_{n,b} = \frac{n+bN}{f_s} - \frac{2R_i}{c}. \tag{2.30}$$

As a first approximation, we assume that the coherent sum is identical across all batches in the CPI, *i.e.*, $S_b \approx S$ for all $b = 0, 1, \ldots, B-1$. Then, the remaining effect of a moving target is that the phase evolves by $\exp\left[2\pi \mathrm{i} \frac{N f_\mathrm{D}}{f_s}\right]$ between batches. This means that the slow-time coherent sum along row $i$ can be computed as

$$\sum_{b=0}^{B-1} \left[\mathbf{C}\right]_{i,b} \exp\left[-2\pi \mathrm{i} N b \frac{f_\mathrm{D}}{f_s}\right] = \theta S B, \tag{2.31}$$

*i.e.*, an effective increase in the signal strength of $B$. When computing a grid of velocities, the slow-time coherent sum can be implemented with a Fourier transform along the rows of $\mathbf{C}$ as

$$\mathbf{Z} = \mathcal{F}_{\rightarrow}\left[\mathbf{C}\right]. \tag{2.32}$$

### 2.3.1 Target movement compensation

If the target is stationary, the fast-time sum of Eq. (2.29) will be a perfect match between the observed and reference signal and there will be no losses involved in processing the signal in batches compared to the 2D cross-correlation. However, a moving target will induce differences between the reference and observed signals, causing integration losses [68]. With knowledge of $v$, we can apply two operations to mitigate this loss without the need for a full resampling of the reference. The simplest improvement is to apply a Doppler modulation to the reference as

$$\left[\mathbf{x}'\right]_m = \left[\mathbf{x}\right]_m \exp\left[2\pi \mathrm{i} m \frac{f_\mathrm{D}}{f_s}\right], \tag{2.33}$$

which corrects for the phase evolution in Eq. (2.29), and is sufficient when range cell migration is negligible. For faster targets or longer integration times we need to also compensate for time dilation in the baseband signal.

The Fourier transform has the property that a time shift in the time domain corresponds to a phase shift in the frequency domain, as

$$[\mathcal{F}[\mathbf{x}_{m-a}]]_n = [\mathcal{F}[\mathbf{x}_m]]_n \exp\left[-2\pi \mathrm{i}\frac{an}{M}\right]. \tag{2.34}$$

This means we can apply a phase factor in the Fourier domain to approximately correct for time dilation in the baseband waveform. Within the batch processing, this corresponds to shifting each batch by a constant time. Since the Fourier transforms are already implemented for the correlation, time dilation compensation can be implemented simply with an extra phase factor in Eq. (2.26) as

$$\mathbf{c}'_b = \mathcal{F}_{\downarrow}^{-1}\left[\mathcal{F}_{\downarrow}\left[(\mathbf{x}'_b)^*\right] \odot \mathcal{F}_{\downarrow}[\mathbf{y}_b] \odot \boldsymbol{\epsilon}_b\right], \tag{2.35}$$

where the phase factor[2] is

$$[\boldsymbol{\epsilon}_b]_n = \exp\left(-2\pi \mathrm{i} n b \frac{f_\mathrm{D}}{f_c}\right). \tag{2.36}$$

Finally, the correlation grid matched to velocity $v$ is

$$\mathbf{Z}' = \mathcal{F}_{\rightarrow}\left[\mathbf{c}'_0\ \mathbf{c}'_1\ \ldots\ \mathbf{c}'_{B-1}\right]. \tag{2.37}$$

While it mitigates the mismatch losses, computing the correlation grid for a large number of velocities increases the required computational resources. Preferably, the relevant range of possible velocities is covered by computing the correlation grid matched to a set of velocities separated to ensure the integration loss is limited.

### 2.3.2 Correlation noise floor

The correlation noise floor (CNF) is a central effect in noise radar operation. It occurs when there is more than one signal present in the observed data and takes the form of a raised noise floor, approximately the time-bandwidth product beneath the strongest signal. We now derive this effect. Assume that the observed signal contains two signals, well separated in range and velocity with $R_1 \neq R_2$ and $v_1 \neq v_2$, as

$$\mathbf{y} = \theta_1 \mathbf{h}_1 + \theta_2 \mathbf{h}_2, \tag{2.38}$$

where $\mathbf{h}_1 \equiv \mathbf{h}(R_1, v_1)$ and $\mathbf{h}_2 \equiv \mathbf{h}(R_2, v_2)$. As discussed above, one approach to detect signal #1 is to compute the product $z = \mathbf{h}_1^\dagger \mathbf{y}$ and check if the modulus

[2]This expression is found in the inner sum of Eq. (7) in **Paper II**, which has an error that should be corrected as $\mathrm{e}^{2\pi \mathrm{i}\frac{q\cdot p}{M}} \rightarrow \mathrm{e}^{2\pi \mathrm{i}\frac{q\cdot m}{M}}$.

square exceeds a predefined threshold. Since the two signals are well separated, we can model them as independent random vectors distributed as $\mathcal{CN}\left(\mathbf{0}, M^{-1}\mathbb{I}_M\right)$. Then, keeping $\theta_1$ and $\theta_2$ fixed, the expectation value over the modulus square of the correlation is

$$\begin{aligned}
\mathbb{E}\left|z\right|^2 &= \mathbb{E}\left|\theta_1|\mathbf{h}_1|^2 + \theta_2\mathbf{h}_1^\dagger\mathbf{h}_2\right|^2 \\
&= \mathbb{E}\left[|\theta_1|^2|\mathbf{h}_1|^4 + |\theta_2|^2|\mathbf{h}_1^\dagger\mathbf{h}_2|^2 + 2\mathfrak{Re}\left(\theta_1^*\theta_2\mathbf{h}_1^\dagger\mathbf{h}_2\right)\right] \\
&= |\theta_1|^2\mathbb{E}|\mathbf{h}_1|^4 + |\theta_2|^2\mathbb{E}|\mathbf{h}_1^\dagger\mathbf{h}_2|^2 + 2\mathfrak{Re}\left(\theta_1^*\theta_2\mathbb{E}\left[\mathbf{h}_1^\dagger\mathbf{h}_2\right]\right) \\
&= \frac{(M+1)|\theta_1|^2 + |\theta_2|^2}{M},
\end{aligned} \tag{2.39}$$

where we used[3] that $\mathbb{E}\left[|\mathbf{h}_1|^4\right] = \frac{M+1}{M}$, $\mathbb{E}\left[|\mathbf{h}_1^\dagger\mathbf{h}_2|^2\right] = M^{-1}$, and that $\mathbb{E}\left[\mathbf{h}_1^\dagger\mathbf{h}_2\right] = \mathbb{E}\left[\mathbf{h}_1^\dagger\right]\mathbb{E}\left[\mathbf{h}_2\right] = 0$. Eq. (2.39) illustrates how a finite correlation in the modulus square, proportional to $M^{-1}$, between the two independent signals causes sidelobes from the second target to interfere with our test for the first target. Since the distance and velocity of the two targets are arbitrary, we conclude that these stochastic sidelobes will affect *all* possible range and velocity cells. Because of its random nature, this effect can be understood as a raised noise floor.

Let us now require that, to be detected separately from noise, the correlation $\left|\mathbf{h}_1^\dagger\mathbf{y}\right|^2$ must produce a local peak that is stronger than a factor of $\gamma$ relative to the local noise floor. Then, because of the CNF, this corresponds to a requirement that $(M+1)|\theta_1|^2 > \gamma|\theta_2|^2$. If this is not satisfied, the stochastic sidelobes from signal #2 will mask signal #1. This consequence of the CNF is known as the *masking effect* [69].

As an example, consider two signals that are due to reflections off of two identical targets with $R_1 > R_2$. Using Eq. (2.1) for the relative return power, we can estimate that the range that target #1 can be detected must satisfy $R_1 < R_2[(M+1)/\gamma]^{1/4}$. In our setup, we use $M \approx 10^7$ and $\gamma \approx 13.8$ which implies $[(M+1)/\gamma]^{1/4} \approx 30$. Thus, if $R_2 = 10$ m, target #1 can ideally be detected at a distance of $R_1 = 300$ m. In practice, we will always expect clutter within at least 100 m of the radar system, indicating that the masking effect will limit detection ranges to a few kilometres, at best.

While it introduces some challenges, the masking effect can be mitigated by changing how the signal is processed, *e.g.*, by incorporating knowledge of signal #2 in the computation of $\mathbf{Z}$ as we will see below.

[3]For details, see Eq. (A.2) and Eq. (A.3) in the Appendix.

## 2.4 Noise radar detector

So far, we have modelled the signals involved in noise radar operation. In a typical radar scenario, we are ignorant to the presence of possible targets. Instead of directly estimating and reporting all signal coefficients, the radar should report only those signals that are strong enough that confidently can be said to originate from actual targets. The question is whether the observed signal $\mathbf{y}$, of length $M$, originates from thermal noise, or from a target signal plus the thermal noise. This question can be stated as a binary decision where the two hypotheses are

$$\begin{aligned} \mathcal{H}_0 : &\quad \mathbf{y} = \text{noise}, \\ \mathcal{H}_1 : &\quad \mathbf{y} = \theta \cdot \text{signal} + \text{noise}. \end{aligned}$$

Now, we introduce a central function of any radar: the signal detector. Detection is understood mathematically as the indicator function

$$\mathbf{1}_\gamma(\Lambda) = \begin{cases} 1 & \text{if } \Lambda \geq \gamma, \\ 0 & \text{otherwise.} \end{cases} \tag{2.40}$$

The indicator function compares a test statistic $\Lambda \in \mathbb{R}$ with a threshold value $\gamma \in \mathbb{R}$. The test statistic is a function of the observed signal data $\mathbf{y}$, and parameters $\boldsymbol{\alpha}$, labelling the the signal under test, *i.e.*, $\Lambda = \Lambda(\mathbf{y}; \boldsymbol{\alpha})$. The parameters could be distance $R$ and radial velocity $v$, as in Eq. (2.19) and we would have $\boldsymbol{\alpha} = [R, v]^\top$. Indeed, we will implement the detector for range and velocity parameters. However, other parameters such as direction, acceleration, and more could also be included in $\boldsymbol{\alpha}$. If a certain input gives an indication, we interpret that those parameters $\boldsymbol{\alpha}$ can be associated with a signal detected in $\mathbf{y}$.

Regardless of what the threshold is tuned to, the detector will unavoidably be subject to statistical error. For any given problem, the detector can be characterised in terms of the conditional probabilities that it declares the correct (or false) result. In the context of radar, it is conventional to use the events of *True Positive* and *False Positive* outcomes, quantified with the probability of detection $P_\mathrm{D}$ and false alarm $P_\mathrm{FA}$, respectively. Both detection and false alarm refer to the event when the detector declares in favour of target presence, conditioned on whether the target is actually present or not. In the terminology of decision making, the false alarm is a Type-I error and the miss is a Type-II error. A quantity familiar to any radar engineer is the relation between probability of detection and probability of false alarm, given a certain signal-to-noise ratio. This relation is known as a receiver operating characteristic (ROC) and captures how enforcing a low probability of false alarms by raising the threshold necessarily lowers the probability of detection.

As an alternative to studying the trade-off between the Type-I and Type-II errors, there is the related quantity of the total error probability, defined as

$$P_\mathrm{E} = \pi_0 P_\mathrm{FA} + \pi_1 (1 - P_\mathrm{D}), \tag{2.41}$$

where $\pi_0$ and $\pi_1$ are the *a priori* probabilities of the events associated with $\mathcal{H}_0$ and $\mathcal{H}_1$, respectively. The total error is commonly used in the communication scenario, where the priors are known. On the other hand, the prior probabilities are unknown for radar scenarios and the total error probability is not useful.

While simple in concept, there are several challenges in designing a detector. How should the test statistic $\Lambda(\mathbf{y}; \boldsymbol{\alpha})$ be designed and implemented? How to set the threshold $\gamma$? If the threshold is reduced, the radar will be able to find weaker target signals at the cost of an increase in the number of false alarms. Conversely, an increase in the threshold will lower the probability of false alarms, but the radar will be less sensitive to weak target signals.

One simple way to define a binary detector function when the priors are unknown is as a likelihood ratio test [70] (LRT). The LRT takes as input the observation $\mathbf{y}$ and computes the test statistic

$$L_{\mathrm{LRT}} = \frac{p(\mathbf{y} \,|\, \mathcal{H}_1)}{p(\mathbf{y} \,|\, \mathcal{H}_0)}, \tag{2.42}$$

where $p(\mathbf{y}|\mathcal{H}_i)$ denotes the probability density function (PDF) of $\mathbf{y}$ under hypothesis $\mathcal{H}_i$. For practical purposes, the log-likelihood test statistic, $\Lambda_{\mathrm{LRT}} = 2 \log L_{\mathrm{LRT}}$, is often more useful than the direct ratio. It is known that, for many repeated independent and identically distributed measurements, such that the central limit theorem applies, any log-likelihood test is asymptotically distributed as a chi-squared random variable. This result is known as Wilks's theorem [71]. For a *simple* binary hypothesis test, *e.g.*, $\theta = 0$ against $\theta = \theta_1$, where $\theta_1$ is known, the likelihood ratio test is optimal by the Neyman-Pearson Lemma [70]. In a radar scenario, the simple hypothesis is usually not encountered, because the value of $\theta$ is not known. In this case optimality of the likelihood ratio test is not guaranteed. In the general case, is it impossible to find a globally optimal detector function for these problems, and one might have to resort to a locally optimised test.

### 2.4.1 Signal estimation

Before developing the detector in detail, we need to handle our ignorance of the signal coefficient $\theta$. To do this, we specify the signal model and use some results from estimation theory [72]. To combat the CNF issues, we will describe the detector as a problem of detection and rejection of *multiple* signals. The total signal model incorporates one target signal $\mathbf{y}_T = \mathbf{h}_T \theta_T$ according to Eq. (2.19) and clutter signals $\mathbf{y}_C = \mathbf{H}_C \boldsymbol{\theta}_C$ according to Eq. (2.20). At this point, we can no longer postpone the introduction of the system noise $\boldsymbol{\nu}$. The noise is distributed according to the complex normal distribution, *i.e.*, $\boldsymbol{\nu} \sim \mathcal{CN}\left(\mathbf{0}, \sigma^2 \mathbb{I}_M\right)$, with variance $\sigma^2$. In principle, we may model coloured noise with non-diagonal covariance matrix. However, as long as the covariance matrix is known, we could decompose it to pre-

whiten[4] the signals which results in an identity covariance matrix. Thus, there is no limitation imposed by this assumption on the noise.

We write the total observed signal as

$$\begin{aligned}\mathbf{y} &= \mathbf{y}_T + \mathbf{y}_C + \boldsymbol{\nu} \\ &= \underbrace{\begin{bmatrix}\mathbf{h}_T & \mathbf{H}_C\end{bmatrix}}_{\equiv \mathbf{H}} \underbrace{\begin{bmatrix}\theta_T \\ \boldsymbol{\theta}_C\end{bmatrix}}_{\equiv \boldsymbol{\theta}} + \boldsymbol{\nu}.\end{aligned} \tag{2.43}$$

In this formalism, the only distinction between target and clutter is whether the signals are of interest to the radar operator. Mathematically, this corresponds to whether the signal is described by the columns of $\mathbf{h}_T$ or $\mathbf{H}_C$. Beyond that, the signal model is generic and allows for arbitrary columns. We will always assume that the total signal matrix $\mathbf{H} = \begin{bmatrix}\mathbf{h}_T & \mathbf{H}_C\end{bmatrix}$ is a tall matrix (*i.e.*, $P_C + 1 \ll M$) of rank $P_C + 1$, such that the estimation problem is well posed.

For now, we assume that the signal basis (*i.e.*, the matrix $\mathbf{H}$) are known, but the coefficients $\boldsymbol{\theta}$ is an unknown vector of length $P_C + 1$. Then, the coefficients are estimated as

$$T_{\boldsymbol{\theta}} = \left(\mathbf{H}^\dagger \mathbf{H}\right)^{-1} \mathbf{H}^\dagger \mathbf{y}, \tag{2.44}$$

which is the solution to the least-squares problem

$$T_{\boldsymbol{\theta}} = \underset{\boldsymbol{\theta}}{\operatorname{argmin}} \left(\mathbf{y} - \mathbf{H}\boldsymbol{\theta}\right)^\dagger \left(\mathbf{y} - \mathbf{H}\boldsymbol{\theta}\right). \tag{2.45}$$

Here, $T_{\boldsymbol{\theta}}$ denotes an unbiased estimator of the parameters $\boldsymbol{\theta}$, *i.e.*, $\mathbb{E}\left[T_{\boldsymbol{\theta}}\right] = \boldsymbol{\theta}$. In this setting, the clutter amplitudes $\boldsymbol{\theta}_C$ are nuisance parameters – additional unknowns that we must account for in the estimation task, even though our primary interest may be $\theta_T$.

The structure of the problem may be elucidated by extracting the estimate for the target parameters alone which, by Eq. (B.6), is

$$T_{\theta_T} = \left[\left(\mathbb{I} - \mathbf{H}_C \mathbf{H}_C^+\right) \mathbf{h}_T\right]^+ \mathbf{y}, \tag{2.46}$$

where $\mathbf{H}_C^+$ is the Moore-Penrose *pseudoinverse*. It is notationally convenient to introduce the projection matrices $\mathbf{P}_{\mathbf{H}_C} = \mathbf{H}_C \mathbf{H}_C^+$ and $\mathbf{P}_{\mathbf{H}_C}^\perp = \mathbb{I} - \mathbf{P}_{\mathbf{H}_C}$. In this form, the estimate (2.46) can be interpreted as the least-squares fit of the data

[4]Thermal noise is always full rank and its covariance matrix $\boldsymbol{\Sigma}$ is guaranteed to be non-singular. We may decompose the inverse covariance matrix as $\boldsymbol{\Sigma}^{-1} = \mathbf{D}^\dagger \mathbf{D}$ and define the *pre-whitened* observed signal and observation matrix, as $\tilde{\mathbf{y}} = \mathbf{D}\mathbf{y}$ and $\tilde{\mathbf{H}} = \mathbf{D}\mathbf{H}$, respectively. After this transformation, the noise is white, since $\mathbf{D}\boldsymbol{\nu} \sim \mathcal{CN}(\mathbf{0}, \mathbb{I})$.

to the target signal in the subspace that is orthogonal to the subspace of clutter signals. Then, Eq. (2.46) can be understood as the 'clutter-free' scalar product

$$T_{\theta_T} = \frac{\mathbf{h}_T^\dagger \mathbf{P}_{\mathbf{H}_C}^\perp \mathbf{y}}{||\mathbf{P}_{\mathbf{H}_C}^\perp \mathbf{h}_T||^2}. \tag{2.47}$$

In the absence of clutter, the estimate reduces to $T_{\theta_T} = \mathbf{h}_T^\dagger \mathbf{y}$, which is the scalar product considered in Section 2.3.

### 2.4.2 Detector function

We form our detection problem as a binary hypothesis test based on the signal model of Eq. (2.43). The null hypothesis $\mathcal{H}_0$ has $P_C$ signals described by $\mathbf{H}_C$ and the alternative hypothesis $\mathcal{H}_1$ has $P_C + 1$ signals jointly described by $\mathbf{h}_T = \mathbf{h}_T(\boldsymbol{\alpha})$ and $\mathbf{H}_C$. We state the two hypotheses as

$$\begin{aligned} \mathcal{H}_0 : &\quad \mathbf{y} = \mathbf{H}_C \boldsymbol{\theta}_C + \boldsymbol{\nu} \sim \mathcal{CN}\left(\mathbf{H}_C \boldsymbol{\theta}_C, \boldsymbol{\Sigma}\right) \\ \mathcal{H}_1 : &\quad \mathbf{y} = \mathbf{h}_T \theta_T + \mathbf{H}_C \boldsymbol{\theta}_C + \boldsymbol{\nu} \sim \mathcal{CN}\left(\mathbf{h}_T \theta_T + \mathbf{H}_C \boldsymbol{\theta}_C, \boldsymbol{\Sigma}\right) \end{aligned} \tag{2.48}$$

with $||\theta_T||^2 > 0$. The formalism used to analyse this hypothesis test results in what is known as the *Matched subspace detector* [73]. We use the total observation matrix $\mathbf{H} = \begin{bmatrix} \mathbf{h}_T & \mathbf{H}_C \end{bmatrix}$ when referring to the signals involved in the alternative hypothesis. The derivation of this result as presented here is well known and can be found in textbooks, see, *e.g.*, Ref. [70].

To define the test statistic, we use the *generalised* likelihood ratio test (GLRT). We consider the case where the detector is adaptive against white noise with unknown variance, *i.e.*, we assume the noise covariance matrix is diagonal, $\boldsymbol{\Sigma} = \sigma^2 \mathbb{I}$, but the scaling $\sigma^2$ is unknown[5]. In this form, the GLRT will have the *scale-invariance* property in the sense that the test will be independent of the true value of $\sigma^2$.

The generalised likelihood ratio $\Lambda'(\mathbf{y})$ applies the LRT of Eq. (2.42) and replaces the unknown parameters with their corresponding maximum likelihood estimators, as

$$\Lambda'(\mathbf{y}) = \frac{p\left(\mathbf{y}|\mathcal{H}_1, T_{\boldsymbol{\theta}}, T_{\sigma_1^2}\right)}{p\left(\mathbf{y}|\mathcal{H}_0, T_{\boldsymbol{\theta}_C}, T_{\sigma_0^2}\right)}, \tag{2.49}$$

where $T_{\sigma_0^2}$ and $T_{\sigma_1^2}$ are the variance estimators under the respective hypotheses, to be determined. Letting the unknown variance estimates be fixed for a moment, we have that $T_{\boldsymbol{\theta}}$ is given in Eq. (2.44). Inserting the expression of Eq. (2.44) in the PDF of $\mathcal{H}_1$ we get

$$p\left(\mathbf{y}|\mathcal{H}_1, T_{\boldsymbol{\theta}} = \mathbf{H}^+\mathbf{y}, T_{\sigma_1^2}\right) = \frac{\exp\left[-||\mathbf{P}_{\mathbf{H}}^\perp \mathbf{y}||^2 / T_{\sigma_1^2}\right]}{\pi^M T_{\sigma_1^2}^M}. \tag{2.50}$$

[5]This is equivalent to $\boldsymbol{\Sigma} = \sigma^2 \boldsymbol{\Sigma}_0$, where the structure $\boldsymbol{\Sigma}_0$ is known, if the signals are pre-whitened with respect to $\boldsymbol{\Sigma}_0$.

Now, we find the maximum likelihood estimate $T_{\sigma_1^2}$ by maximising the PDF, which is equivalent to minimising its negative logarithm, such that

$$\begin{aligned} T_{\sigma_1^2} &= \underset{T_{\sigma_1^2}}{\operatorname{argmax}} \frac{\exp\left[-||\mathbf{P}_{\mathbf{H}}^{\perp}\mathbf{y}||^2/T_{\sigma_1^2}\right]}{\pi^M T_{\sigma_1^2}^M} \\ &= \underset{T_{\sigma_1^2}}{\operatorname{argmin}} \left[M\pi + M\ln T_{\sigma_1^2} + \frac{||\mathbf{P}_{\mathbf{H}}^{\perp}\mathbf{y}||^2}{T_{\sigma_1^2}}\right] \\ &= \underset{T_{\sigma_1^2}}{\operatorname{argmin}} \left[\ln T_{\sigma_1^2} + \frac{||\mathbf{P}_{\mathbf{H}}^{\perp}\mathbf{y}||^2}{MT_{\sigma_1^2}}\right], \end{aligned} \tag{2.51}$$

with the solution $T_{\sigma_1^2} = \frac{||\mathbf{P}_{\mathbf{H}}^{\perp}\mathbf{y}||^2}{M}$. By repeating the same steps for $\mathcal{H}_0$, we find $T_{\sigma_0^2} = \frac{||\mathbf{P}_{\mathbf{H}_C}^{\perp}\mathbf{y}||^2}{M}$. The concentrated PDFs under either hypothesis are

$$p\left(\mathbf{y}|\mathcal{H}_1, T_{\boldsymbol{\theta}} = \mathbf{H}^{+}\mathbf{y}, T_{\sigma_1^2} = \frac{||\mathbf{P}_{\mathbf{H}}^{\perp}\mathbf{y}||^2}{M}\right) = \frac{M^M \mathrm{e}^{-M}}{\pi^M ||\mathbf{P}_{\mathbf{H}}^{\perp}\mathbf{y}||^{2M}} \tag{2.52}$$

and

$$p\left(\mathbf{y}|\mathcal{H}_0, T_{\boldsymbol{\theta}_C} = \mathbf{H}_C^{+}\mathbf{y}, T_{\sigma_0^2} = \frac{||\mathbf{P}_{\mathbf{H}_C}^{\perp}\mathbf{y}||^2}{M}\right) = \frac{M^M \mathrm{e}^{-M}}{\pi^M ||\mathbf{P}_{\mathbf{H}_C}^{\perp}\mathbf{y}||^{2M}}. \tag{2.53}$$

With the concentrated PDFs, the GLRT statistic of Eq. (2.49) simplifies to

$$\Lambda'(\mathbf{y}) = \left(\frac{||\mathbf{P}_{\mathbf{H}_C}^{\perp}\mathbf{y}||^2}{||\mathbf{P}_{\mathbf{H}}^{\perp}\mathbf{y}||^2}\right)^M. \tag{2.54}$$

We get a simpler form of a fully equivalent test by taking the $M$'th root and subtracting 1, as $\Lambda''(\mathbf{y}) = (\Lambda'(\mathbf{y}))^{1/M} - 1$. Then, with some subsequent simplifications, we have

$$\begin{aligned} \Lambda''(\mathbf{y}) &= \frac{||\mathbf{P}_{\mathbf{H}_C}^{\perp}\mathbf{y}||^2}{||\mathbf{P}_{\mathbf{H}}^{\perp}\mathbf{y}||^2} - 1 \\ &= \frac{\mathbf{y}^{\dagger}\left[\mathbf{P}_{\mathbf{H}_C}^{\perp} - \mathbf{P}_{\mathbf{H}}^{\perp}\right]\mathbf{y}}{||\mathbf{P}_{\mathbf{H}}^{\perp}\mathbf{y}||^2} \\ &= \frac{\mathbf{y}^{\dagger}\left[\mathbf{P}_{\mathbf{H}} - \mathbf{P}_{\mathbf{H}_C}\right]\mathbf{y}}{\mathbf{y}^{\dagger}\left[\mathbf{P}_{\mathbf{H}_C}^{\perp} - \mathbf{P}_{\check{\mathbf{h}}_T}\right]\mathbf{y}} \\ &= \frac{\mathbf{y}^{\dagger}\mathbf{P}_{\check{\mathbf{h}}_T}\mathbf{y}}{||\mathbf{P}_{\mathbf{H}_C}^{\perp}\mathbf{y}||^2 - \mathbf{y}^{\dagger}\mathbf{P}_{\check{\mathbf{h}}_T}\mathbf{y}} \\ &= \frac{|\mathbf{h}_T^{\dagger}\mathbf{P}_{\mathbf{H}_C}^{\perp}\mathbf{y}|^2}{||\mathbf{P}_{\mathbf{H}_C}^{\perp}\mathbf{h}_T||^2||\mathbf{P}_{\mathbf{H}_C}^{\perp}\mathbf{y}||^2 - |\mathbf{h}_T^{\dagger}\mathbf{P}_{\mathbf{H}_C}^{\perp}\mathbf{y}|^2}, \end{aligned} \tag{2.55}$$

where $\check{\mathbf{h}}_T = \mathbf{P}^{\perp}_{\mathbf{H}_C}\mathbf{h}_T$ and where we used Eq. (B.5) for the projection matrix of a concatenated matrix.

A hypothesis test statistic like the GLRT is by necessity a random variable and characterisation of the probability distribution is central to its usefulness. So far, we have not said anything about the distribution of $\Lambda''$. Following the steps of Ref. [73] we note that $\Lambda''$ satisfies the form of a ratio between two independent chi-squared random variables, missing only a scaling with 2 and $2M - 2P_C - 2$ degrees of freedom in the numerator and denominator, respectively. Such a ratio is distributed according to the $F$ distribution [70, 74]. By multiplying $\Lambda''$ by $\frac{2M-2P_C-2}{2}$, we arrive at our final test function

$$\Lambda(\mathbf{y}) = \frac{(M - P_C - 1)\,|\mathbf{h}_T^{\dagger}\mathbf{P}^{\perp}_{\mathbf{H}_C}\mathbf{y}|^2}{||\mathbf{P}^{\perp}_{\mathbf{H}_C}\mathbf{h}_T||^2||\mathbf{P}^{\perp}_{\mathbf{H}_C}\mathbf{y}||^2 - |\mathbf{h}_T^{\dagger}\mathbf{P}^{\perp}_{\mathbf{H}_C}\mathbf{y}|^2}. \tag{2.56}$$

The test statistic has the statistical properties[6]

$$\Lambda(\mathbf{y}) \sim \begin{cases} F_{2,2M-2P_C-2} & \text{under } \mathcal{H}_0, \\ F_{2,2M-2P_C-2}\left(\lambda^2\right) & \text{under } \mathcal{H}_1. \end{cases} \tag{2.57}$$

Under $\mathcal{H}_1$, the non-centrality parameter is

$$\lambda^2 = \frac{|\theta_T|^2}{\sigma^2}||\mathbf{P}^{\perp}_{\mathbf{H_C}}\mathbf{h}_T||^2, \tag{2.58}$$

which can be understood as the power signal-to-noise ratio (SNR) in the clutter-free subspace. Under $\mathcal{H}_0$, $\Lambda$ is independent of the unknown parameters, and any threshold $\gamma$ will specify a certain probability of false alarm according to $P_{\text{FA}} = \Pr\left[\Lambda\left(\mathbf{y}\right) \geq \gamma|\mathcal{H}_0\right]$. That is, a detector using $\Lambda$ as the test statistic is said to have the constant false alarm rate (CFAR) property. In many radar settings, the threshold may be designed according to a desired rate of false alarms. Mathematically, we can approach such a threshold tuning by first computing the right-tail marginal distribution of $\Lambda$ under the null hypothesis, as

$$\begin{aligned} P_{\text{FA}} &= \int_{\gamma}^{\infty} \mathrm{d}s\, p_{F_{2,2M-2P_C-2}}(s) \\ &= \left(1 + \frac{\gamma}{M - P_C - 1}\right)^{-M+P_C+1}, \end{aligned} \tag{2.59}$$

where the PDF $p_{F_{2,2M-2P_C-2}}(s)$ is presented in Eq. (A.5). By solving the result for $\gamma$ we get the designed CFAR threshold

$$\begin{aligned} \gamma\left(P_{\text{FA}}\right) &= (M - P_C - 1)\left[\exp\left(-\frac{\ln P_{\text{FA}}}{M - P_C - 1}\right) - 1\right] \\ &= -\ln P_{\text{FA}}\left[1 - \frac{\ln P_{\text{FA}}}{2\left(M - P_C - 1\right)}\right] + \mathcal{O}\left[\left(\frac{\ln P_{\text{FA}}}{M - P_C - 1}\right)^3\right]. \end{aligned} \tag{2.60}$$

[6]See Appendix A for some properties of the $F$ distribution.

In our setting, $M \gg P_C + 1$ and the threshold can be set according to $\gamma\left(P_{\mathrm{FA}}\right) = -\ln P_{\mathrm{FA}}$. Often, we are testing for signals that are reasonably well separated from the clutter subspace, in distance or velocity, and we approximate $||\mathbf{P}^{\perp}_{\mathbf{H}_C}\mathbf{h}_T||^2 = 1 - \mathcal{O}\left(M^{-1}\right) \approx 1$, which somewhat simplifies $\Lambda$.

## 2.5 Clutter suppression

In the derivation of the GLRT, we ended up with the test statistic of Eq. (2.56), where the central quantity is the clutter-free scalar product $\mathbf{h}_T^{\dagger}\mathbf{P}^{\perp}_{\mathbf{H}_C}\mathbf{y}$. This may appear to conflict with the processing described in Section 2.3 where $\mathbf{h}_T^{\dagger}\mathbf{y}$ was considered. However, the processing is identical when applied to the clutter-free observation vector $\check{\mathbf{y}} = \mathbf{P}^{\perp}_{\mathbf{H}_C}\mathbf{y}$. In this section, we briefly present some possible approaches to computing $\check{\mathbf{y}}$ as pre-processing step, collectively referred to as clutter suppression algorithms. The algorithms discussed here are those that appear in the appended papers, but there are several other approaches [75–78].

Our main reason for considering clutter suppression is that those signals often are significantly stronger than the signals of targets of interest. In several settings, and for continuous transmission in particular, the CNF from clutter[7] will dominate. If $\mathbf{H}_C$ is an accurate representation of the clutter environment and its columns span the strongest signals in the observation vector, correlation processing on $\check{\mathbf{y}}$ will be free of the CNF. Of course, there are several reasons why this is an unattainable ideal, and some residual impact of the CNF will always remain. One limitation is that we model the signal coefficients as constant over the CPI – an assumption that may fail in reality. There may also be signals outside span of $\mathbf{H}_C$ that we fail to account for.

Regarding the computation of $\check{\mathbf{y}}$, we can imagine two types of algorithms. In the first type, $\mathbf{H}_C$ is supplied to the algorithm based on a clutter map, where each column is known or expected to represent a strong signal based on previous knowledge. In the second type, the columns of $\mathbf{H}_C$ are populated automatically during the pre-processing step, *e.g.*, by iteration. In some sense, these two types can be understood as non-adaptive and adaptive, respectively.

When considering these types of algorithms, two design choices that become relevant are:

- The model order $P_C$, *i.e.*, the number of columns in $\mathbf{H}_C$;
- The *dictionary* $\{\mathbf{h}_d\}$, *i.e.*, the *possible* columns that we may add to $\mathbf{H}_C$.

The dictionary $\{\mathbf{h}_d\} = \{\mathbf{h}_d : d = 0, 1, \ldots\}$ can be quite arbitrary in general, and the procedures hold for both on-grid (discrete dictionary) and off-grid (continuous

[7] In this sense, clutter be can reflections from objects in the environment, but also near-field coupling between transmitter and receiver antennas, or direct signal interference in a bistatic configuration.

dictionary) methods. As we have noted before, the dictionary vectors $\mathbf{h}_d$ could be parameterised with respect to range, velocity, direction, etc. However, we will continue with the assumption that $\{\mathbf{h}_d\}$ is a finite set of vectors on a range-velocity grid. Without loss of generality, we assume that all vectors in the dictionary are normalised, *i.e.*, $||\mathbf{h}_d||^2 = 1$ for all $d$. We do not require the dictionary vectors to be mutually orthogonal, since the computation of such dictionary would not be viable with the length of vectors and size of the range-velocity grid we consider. However, with noisy waveforms, our dictionary contains vectors that are almost mutually orthogonal, as $|\mathbf{h}_d^\dagger \mathbf{h}_d'|^2 \approx M^{-1}$ for $d \neq d'$. We continue to assume that the noise covariance matrix is diagonal, as in the case with thermal noise. At this point, it is important to emphasise that the projection matrix $\mathbf{P}_{\mathbf{H}_C}^\perp$ is convenient for compact notation, but should generally not be formed explicitly since it requires $\mathcal{O}(P_C^2 M)$ number of operations to compute and memory of size $\mathcal{O}(M^2)$.

### 2.5.1 CLEAN

The CLEAN algorithm[8] is a 'greedy' [80] procedure that investigates the observed signals by iteration. It works by repeating the following three steps

1. Identify the strongest signal in the data as $\mathbf{h}' = \text{argmax}_{\{\mathbf{h}_d\}} |\mathbf{h}_d^\dagger \mathbf{y}|^2$;
2. Estimate the coefficient of the strongest signal: $T_{\theta'}$ for $\mathbf{h}'$;
3. Subtract the strongest signal from the data: $\mathbf{y} \leftarrow \mathbf{y} - \mathbf{h}' T_{\theta'}$.

Step 3 can be stated as the projection $\mathbf{y} \leftarrow \mathbf{P}_{\mathbf{h}'}^\perp \mathbf{y}$. Thus, the output of this procedure is a data vector that approximates $\check{\mathbf{y}}$, where the columns of $\mathbf{H}_C$ are the vectors $\mathbf{h}'$ from all the iterations. However, since CLEAN keeps no memory of previous $\mathbf{h}'$, performance will degrade if there is even a small overlap between iterations. For example, the amplitude of the coefficient may be overestimated in early iterations due to the CNF. An incorrect estimate $T_{\theta'}$ causes the algorithm to accumulate a mismatch over time that eventually leads to saturation, *i.e.*, total energy in the data is no longer reduced by further iterations. CLEAN performance will deteriorate if the model of the strongest signal $\mathbf{h}'$ is incorrect, for example due to stretch effects or system non-linearity.

In **Paper I** we extended CLEAN[9] to account for straddling and extended clutter, *i.e.*, signals that originate off-grid or fail to be point-like. Like before, the strongest signal is identified, but instead of subtracting only the strongest signal, an orthogonal basis including neighbouring cells is used. The joint signal in all of these cells is subtracted from the data. In particular, the algorithm repeats the following steps:

[8] In the original reference, 'CLEAN' is written in all capital letters, but it is not an abbreviation [79].

[9] We referred to the extension as Sequential CLEAN which is misleading. The correct name is Extended CLEAN or Multi-Signal CLEAN.

1. Identify the strongest signal in the data as $\mathbf{h}' = \text{argmax}_{\{\mathbf{h}_d\}} |\mathbf{h}_d^\dagger \mathbf{y}|^2$;
2. Create the signal matrix $\mathbf{H}' = \left[\mathbf{h}', \mathbf{h}_1'', \mathbf{h}_2'', \ldots, \mathbf{h}_Q''\right]$ where $\mathbf{h}_1'', \mathbf{h}_2'', \ldots, \mathbf{h}_Q''$ are perturbations of $\mathbf{h}'$;
3. Estimate $Q+1$ coefficients by $T_{\boldsymbol{\theta}'}$ for $\mathbf{H}'$;
4. Subtract the region of the strongest signal from the data $\mathbf{y} \leftarrow \mathbf{y} - \mathbf{H}' T_{\boldsymbol{\theta}'}$.

At Step 3, it is possible to remove columns of $\mathbf{H}'$ for which the amplitude is negligible and recompute $T_{\boldsymbol{\theta}'}$. In our application with clutter in noise radar, this version of CLEAN worked very well for reducing the correlation noise floor, but created some artefacts around regions where signals had been subtracted, see **Paper I**.

It remains to select a stopping criterion that determines when CLEAN should terminate to prevent it from identifying side-lobes or thermal noise fluctuations as proper signals. A common criterion is to stop iterating when the energy in the signal is no longer sufficiently reduced in the next step. As an alternative, we suggest replacing the matched filter of Step 1 with the detector statistic $\Lambda$ of Eq. (2.56). The algorithm is then allowed to run until the strongest signal $\mathbf{h}'$ is weak enough to fall below the detection threshold. If there are remaining signals that fall below the threshold, they are sufficiently weak to have negligible impact on the CNF. The scale-invariance property of the GLRT makes this version of the algorithm robust against model order runaway, as residual energy will be treated as a raised noise floor and the test statistic scaled accordingly.

We can improve on CLEAN by incorporating the knowledge of removed signals into future iterations. Instead of discarding the selected vector $\mathbf{h}'$ at each iteration we can append it to the matrix $\mathbf{H}_C$, which is initialised empty. Then, the coefficients estimated at previous iterations may be updated as the model order increases. This extension of the algorithm is a version of Orthogonal Matching Pursuit (OMP) [81]. While it introduces extra computations compared to CLEAN, OMP can be implemented relatively efficiently [82].

### 2.5.2 Extensive Cancellation Algorithm

The Extensive Cancellation Algorithm (ECA) [20, 83] is another algorithm that can be used for noise radar processing. ECA requires the clutter observation matrix $\mathbf{H}_C$ to be supplied. Similarly to CLEAN, the central idea of ECA is to use the estimate of the clutter coefficients $T_{\boldsymbol{\theta}_C}$ and subtract the corresponding clutter signals from the observed data vector. We can write this as

$$\mathbf{y}_{\text{ECA}} = \mathbf{y} - \mathbf{H}_C T_{\boldsymbol{\theta}_C}. \tag{2.61}$$

In this form, ECA can be seen as a one-step extended CLEAN, where all the signals defined by $\mathbf{H}_C$ are removed jointly. Because all signals are treated at the same time, there is no problem if they are not mutually orthogonal.

Direct implementation according to Eq (2.61) may require large amounts of computational resources if the model order is large. A significant simplification can be achieved in the case when the clutter is restricted to a limited subspace. Let the clutter be stationary ($v_p = 0$, for $p = 1, 2, \ldots, P_C$), such that the scattering process is simply a delay of the transmitted signal. Assume further that for *each* sample delay the clutter signal's amplitude is non-zero. In this example, the observation matrix is

$$\mathbf{H}_C = \begin{bmatrix} \mathbf{h}\,(0,0) & \mathbf{h}\,(\Delta R, 0) & \mathbf{h}\,(2\Delta R, 0) & \ldots \end{bmatrix}, \tag{2.62}$$

where $\Delta R$ is the range cell size. Eq. (2.62) is a Toeplitz matrix consisting of delayed copies of the reference signal $\mathbf{x}$ up to some maximum relevant delay. Note that the clutter estimate satisfies $\mathbf{H}_C^{\dagger}\mathbf{H}_C T_{\boldsymbol{\theta}_C} = \mathbf{H}_C^{\dagger}\mathbf{y}$ where $\mathbf{H}_C^{\dagger}\mathbf{H}_C$ approximates a Toeplitz matrix of the transmitted signal's autocorrelation $r_x$ and $\mathbf{H}_C^{\dagger}\mathbf{y}$ approximates the cross-correlation between the transmitted and observed signal $r_{xy}$. Thus $T_{\boldsymbol{\theta}_C}$ can be determined from the linear system

$$\begin{bmatrix} r_x(0) & r_x^*(1) & r_x^*(2) & \ldots \\ r_x(1) & r_x(0) & r_x^*(1) & \ldots \\ \vdots & \ddots & \ddots & \ddots \end{bmatrix} T_{\boldsymbol{\theta}_C} = \begin{bmatrix} r_{xy}(0) \\ r_{xy}(1) \\ r_{xy}(2) \\ \vdots \end{bmatrix}. \tag{2.63}$$

In this form, the estimation task can be understood as an optimal filtering problem and is convenient for application in noise radar processing for several reasons. Since the transmitted signal is modelled as a stationary process, its autocorrelation function can be pre-computed, and the cross-correlation with the observed signal is efficiently computed with FFTs, as described earlier. Secondly, the maximum delay considered in Eq. (2.63) can be small relative to the total processing length. For a ground-based noise radar system, this is certainly true, because close-range clutter will cause the most severe contributions to the CNF. Finally, the Toeplitz problem can be efficiently solved with Levinson recursion [84].

## 2.6 Array processing

So far we have modelled the noise radar in the temporal domain, but a radar should preferably also be able to determine the direction to the target. This can be done by sweeping a highly directive antenna, with the result that, as an example, each CPI corresponds to a different direction. In our case, we use a non-rotating array antenna, where direction is determined by comparing the signal from several receiver elements. In particular, we use a receiver antenna in the form of a uniform linear array (ULA) of 8 approximately isotropic antenna elements, and the signal from each element is digitised. The transmitter antenna is smaller, illuminating the scene with a wide lobe. If the transmitter and receiver are operating from the same site, we have a quasi-monostatic setup, but they may be separated for

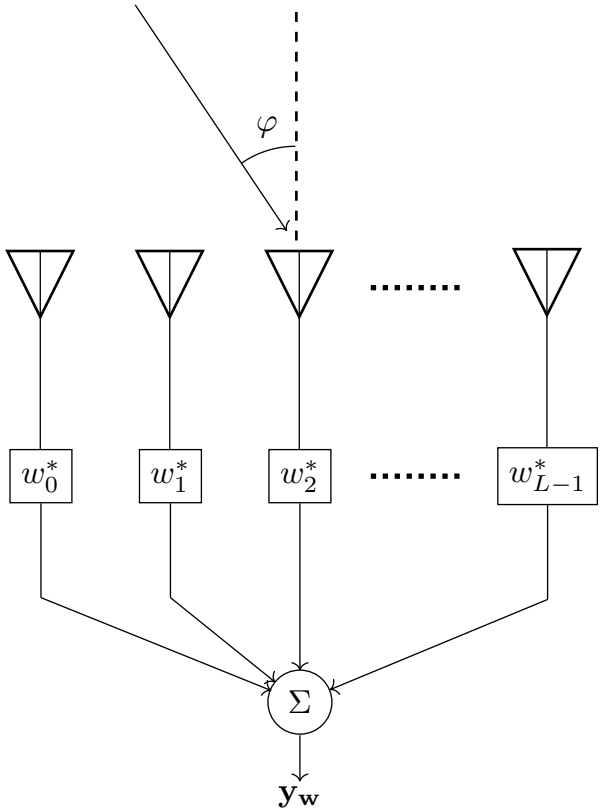


**Figure 2.2:** Schematic overview of a ULA with $L$ antenna elements. A signal is impinging on the array from the direction $\varphi$. The signal is received at each element and multiplied by a channel weight $w_l$. The array output $\mathbf{y_w}$ is the coherent sum from all elements.

bistatic operation. The model used to describe the spatial signals follows in broad terms the presentation of Ref. [85].

### 2.6.1 Target Signal

We consider an ULA antenna in horizontal orientation, consisting of $L$ elements spaced by distance $d$ and labelled by index $l$. Assume that the array picks up the RF signal $y_{\mathrm{RF}}(t)$ of Eq. (2.6) from azimuthal direction $\varphi$ relative the antenna normal, see Fig. 2.2. We assume that the source is far away and that $\varphi$ is constant over the observation interval. If we set the reference time with respect to element $l = 0$ in the array, the instantaneous snapshot of the received signal for element $l$ is $y_{\mathrm{RF}}\left(t - l\frac{d}{c}\sin\varphi\right)$ where $\frac{d}{c}\sin\varphi$ is the inter-element time delay. By using the temporal model from Subsection 2.2.1, we have, as a generalisation of Eq. (2.18), a *spatio-temporal* description of the signal vector[10] $\mathbf{h}(R, v, \varphi)$, of length $ML$, with

[10]While the two discrete indices $m$ and $l$ invites the notion that $\mathbf{h}(R, v, \varphi)$ may be written as a matrix, we shall avoid that convention, because the matrix form is used to describe *multiple* signals, as in Eq. (2.20).

the elements

$$
\begin{aligned}
[\mathbf{h}(R,v,\varphi)]_{m+Ml} = x\left[\left(1+\frac{f_\mathrm{D}}{f_c}\right)\left(\frac{m}{f_s}-\frac{2R_0}{c}\right)-l\frac{d}{c}\sin\varphi\right]\times \\
\exp\left[2\pi\mathrm{i}\left(m\frac{f_\mathrm{D}}{f_s}-lf_c\frac{d}{c}\sin\varphi\right)\right].
\end{aligned}
\tag{2.64}
$$

To ensure that the direction $\varphi$ can be determined unambiguously, the elements must be separated sufficiently close to avoid aliasing, which is satisfied for separation no larger than $d = \frac{\lambda}{2}$ for the RF wavelength $\lambda = \frac{c}{f_c}$. Using this element separation, we have $\frac{d}{c} = \frac{1}{2f_c}$.

Now, we make the crucial assumption that the baseband signal $x$ varies sufficiently slowly to be approximately constant over the array at each snapshot in time. This is a narrowband assumption that holds as long as the bandwidth of $x$ is not too large with respect to the size of the array. The assumption holds if $LB \ll f_c$, where $B$ is the bandwidth of $x$. Under this assumption, we may drop the $l$-dependent term in the baseband as

$$
x\left[\left(1+\frac{f_\mathrm{D}}{f_c}\right)\left(\frac{m}{f_s}-\frac{2R_0}{c}\right)-\frac{l}{2f_c}\sin\varphi\right] = x\left[\left(1+\frac{f_\mathrm{D}}{f_c}\right)\left(\frac{m}{f_s}-\frac{2R_0}{c}\right)\right], \tag{2.65}
$$

for $l = 0, 1, \ldots, L-1$. Then, the spatio-temporal signal vector factorises as

$$
\mathbf{h}(R,v,\varphi) = \mathbf{g}(\varphi)\otimes\mathbf{h}(R,v), \tag{2.66}
$$

where $\mathbf{g}(\varphi)$ is the *spatial* signal vector with elements

$$
\begin{aligned}
[\mathbf{g}(\varphi)]_l &= \exp\left[-2\pi\mathrm{i}lf_c\frac{d}{c}\sin\varphi\right] \\
&= \exp\left[-\pi\mathrm{i}l\sin\varphi\right]
\end{aligned}
\tag{2.67}
$$

for $l = 0, 1, \ldots, L-1$. In summary, the received target signal is modelled as

$$
\mathbf{y} = \theta'\,\mathbf{g}(\varphi)\otimes\mathbf{h}(R,v), \tag{2.68}
$$

which is a spatial extension to the model in Eq. (2.19).

### 2.6.2 Interference

Let us now introduce the possibility that the receiver picks up signals other than our own. We refer to any such signal as *interference*. As a model, we assume that, temporally, the interfering signal $\mathbf{i}$ behaves similarly to noise and is distributed according to the complex normal distribution, $\mathbf{i} \sim \mathcal{CN}\left(\mathbf{0}, |\phi_I|^2\mathbb{I}_M\right)$, where $|\phi_I|^2$ is the average power. Although noise-like from sample-to-sample, any interference will have a finite bandwidth, and we assume that the interfering signal is spatially correlated across the receiver array, as with the target model above. We write the interfering signal, impinging from direction $\varphi_I$, as

$$
\mathbf{j}(\varphi_\mathrm{I}) = \mathbf{g}(\varphi_\mathrm{I})\otimes\mathbf{i}, \tag{2.69}
$$

where $\mathbf{g}(\varphi_{\mathrm{I}})$ is given in Eq. (2.67). Since $\mathbf{i}$ is a random vector, $\mathbf{j}$ characterised by the covariance matrix

$$\mathbb{E}\left[\mathbf{j}(\varphi_{\mathrm{I}})\mathbf{j}^{\dagger}(\varphi_{\mathrm{I}})\right] = |\phi_I|^2\mathbf{G}(\varphi_{\mathrm{I}}) \otimes \mathbb{I}_M, \tag{2.70}$$

where we introduced the rank-1 matrix $\mathbf{G}(\varphi_{\mathrm{I}}) = \mathbf{g}(\varphi_{\mathrm{I}})\mathbf{g}^{\dagger}(\varphi_{\mathrm{I}})$.

### 2.6.3 Total signal model

Now, we are ready to state the total spatio-temporal (ST) signal model as an extension to Eq. (2.43). It incorporates the possibility of $P$ signal sources and $Q$ independent sources of interference as well as internal noise. Explicitly, the observed signal from $M$ samples in $L$ elements is

$$\mathbf{y}_{\mathrm{ST}} = \mathbf{H}_{\mathrm{ST}}\boldsymbol{\theta} + \mathbf{J}\boldsymbol{\phi} + \boldsymbol{\nu}_{\mathrm{ST}}, \tag{2.71}$$

where $\mathbf{H}_{\mathrm{ST}}$ and $\mathbf{J}$ are matrices with columns of Eq. (2.66) and Eq. (2.69), respectively, such that

$$\mathbf{H}_{\mathrm{ST}}\boldsymbol{\theta} = \sum_{p=0}^{P-1}[\boldsymbol{\theta}]_p\mathbf{g}(\varphi_p) \otimes \mathbf{h}(R_p, v_p) \tag{2.72}$$

and

$$\mathbf{J}\boldsymbol{\sigma} = \sum_{q=0}^{Q-1}[\boldsymbol{\phi}]_q\mathbf{g}(\varphi_q) \otimes \mathbf{i}_q. \tag{2.73}$$

The noise is modelled according to $\boldsymbol{\nu}_{\mathrm{ST}} \sim \mathcal{CN}\left(\mathbf{0}, \sigma^2\mathbb{I}_{ML}\right)$, *i.e.*, each array element is subject independent thermal noise with identical variance $\sigma^2$.

Everything we discussed on the topic of temporal signal estimation in Section 2.4 applies equivalently here, with the observed signal distributed as $\mathbf{y}_{\mathrm{ST}} \sim \mathcal{CN}\left(\mathbf{H}_{\mathrm{ST}}\boldsymbol{\theta}, \boldsymbol{\Sigma}_{\mathrm{ST}}\right)$, where the interference-and-noise covariance matrix is

$$\begin{aligned}\boldsymbol{\Sigma}_{\mathrm{ST}} &= \left[\sum_{q=0}^{Q-1}|[\boldsymbol{\phi}]_q|^2\mathbf{G}(\varphi_q)\right] \otimes \mathbb{I}_M + \sigma^2\mathbb{I}_{ML} \\ &= \sigma^2\boldsymbol{\Sigma}_{\mathrm{S}} \otimes \mathbb{I}_M,\end{aligned} \tag{2.74}$$

where

$$\boldsymbol{\Sigma}_{\mathrm{S}} = \sum_{q=0}^{Q-1}\frac{|[\boldsymbol{\phi}]_q|^2}{\sigma^2}\mathbf{G}(\varphi_q) + \mathbb{I}_L \tag{2.75}$$

is the $L \times L$ (normalised) spatial covariance matrix. The normalised weight $|[\boldsymbol{\phi}]_q|^2/\sigma^2$ is the interference-to-noise ratio (INR) of source $q$. By factoring the variance $\sigma^2$, the covariance matrix of Eq. (2.74) is seen to allow for the scale-invariant property of the GLRT, discussed in Section 2.4. Since the covariance matrix is no longer diagonal, the estimation problem is now more complex. However, all the novel statistical properties are captured by the covariance matrix $\boldsymbol{\Sigma}_{\mathrm{S}}$.

### 2.6.4 Adaptive Beamforming

Considering the full spatio-temporal signal processing problem as described by Eq. (2.71) may not be possible because $ML$ data points may not be feasible to process. However, because of the factorised structure, a full space-time treatment is not required and the processing can be performed in simpler steps. Suppose that, as a first step, the signals from each element are coherently summed before further processing, as shown in Figure 2.2, where the $\mathbf{w} = [w_0, w_1, \ldots, w_{L-1}]^\top$ are tuneable channel weights. The spatial degrees of freedom introduced by the channel weights allow us to suppress interfering signals. If the values of $\mathbf{w}$ are not set by the user, but instead tuned according to observed signals, the processing is said to be adaptive. We design the weights to minimise the instantaneous signal power of the output in the case where the input of the array is only interference and noise, denoted

$$\mathbf{y}_{\mathrm{IN}} = \mathbf{J}\boldsymbol{\phi} + \boldsymbol{\nu}_{\mathrm{ST}}, \tag{2.76}$$

and the array output is

$$\mathbf{y}_{\mathrm{IN},\mathbf{w}} = \left(\mathbf{w}^\dagger \otimes \mathbb{I}_M\right) \mathbf{y}_{\mathrm{IN}}. \tag{2.77}$$

Let the $L$-length vector $\bar{\mathbf{y}}_{\mathrm{IN}}(m)$ be the instantaneous signal at each element in the array at the temporal index $m$, defined as

$$[\bar{\mathbf{y}}_{\mathrm{IN}}(m)]_l = [\mathbf{y}_{\mathrm{IN}}]_{m+lM}\,. \tag{2.78}$$

The optimisation problem is

$$\begin{aligned}
\min_{\mathbf{w}} \mathbb{E}\left[ |\,[\mathbf{y}_{\mathrm{IN},\mathbf{w}}]_m\,|^2 \right] &= \min_{\mathbf{w}} \mathbb{E}\left[ \mathbf{w}^\dagger \bar{\mathbf{y}}_{\mathrm{IN}}(m) \bar{\mathbf{y}}_{\mathrm{IN}}^\dagger(m) \mathbf{w} \right] \\
&= \min_{\mathbf{w}} \mathbf{w}^\dagger \mathbb{E}\left[ \bar{\mathbf{y}}_{\mathrm{IN}}(m) \bar{\mathbf{y}}_{\mathrm{IN}}^\dagger(m) \right] \mathbf{w} \\
&= \min_{\mathbf{w}} \mathbf{w}^\dagger \sigma^2 \boldsymbol{\Sigma}_S \mathbf{w} \\
&= \min_{\mathbf{w}} \mathbf{w}^\dagger \boldsymbol{\Sigma}_S \mathbf{w},
\end{aligned} \tag{2.79}$$

where $\boldsymbol{\Sigma}_S$ is the spatial covariance matrix of Eq. (2.75). We must constrain the problem to avoid trivial solutions, with $\mathbf{w} = \mathbf{0}$, which would nullify the array. Therefore, we require that the weights guarantee a fixed sensitivity in look direction $\varphi_0$, as $\mathbf{g}^\dagger(\varphi_0)\mathbf{w} = \beta_0 > 0$. It is possible to introduce more than one constraint here, for example to add artificial nulls to the antenna diagram, and the constraint $\beta_0$ can be selected differently depending on the implementation. This constrained optimisation problem can be solved with Lagrange multipliers. As an example, with the unit scalar constraint ($\beta_0 = 1$), the solution is [85]

$$\mathbf{w}_{\mathrm{opt}} = \frac{\boldsymbol{\Sigma}_S^{-1}\mathbf{g}(\varphi_0)}{\mathbf{g}^\dagger(\varphi_0)\boldsymbol{\Sigma}_S^{-1}\mathbf{g}(\varphi_0)}. \tag{2.80}$$

The spatial covariance matrix will typically be entirely unknown. An *ad hoc* solution to this ignorance is to record data from the array while the transmitter

is inactive, and use an estimated covariance matrix to set the weights. For this method to be viable, the interference environment must be sufficiently stationary that the estimated covariance matrix remains valid when the transmitter is again activated.

### 2.6.5 Wideband effects

So far, we have worked under the assumption that there is no spatial dispersion of the signal across the array. This corresponds to an assumption of the signal being spatially narrowband. Since the ULA can only suppress a number of narrowband signals that is smaller than the degrees of freedom it is important to understand when the narrowband assumption fails. The narrowband assumption is studied in Ref. [86], where it is defined to fail when the second largest eigenvalue of the spatial covariance matrix exceeds the thermal noise.

To quantify wideband effects, we note that the spatial signal vector depends on the carrier frequency $\mathbf{g}(\varphi) = \mathbf{g}(\varphi; f_c)$, see Eq. (2.67). We assume that the expression generalises to an arbitrary frequency $f$ within the system bandwidth. Let one interference source impinge on the array from the direction $\varphi_\mathrm{I}$, covering a bandwidth $B$ centred at $f_c$. For simplicity, let the interference have a constant spectral density $S_\mathrm{I}$. The array response to the interference will not be constant over the entire bandwidth, which means the covariance matrix with respect to this interference will not be rank-1. The interference can be descirbed by the covariance matrix

$$\mathbf{\Sigma}_\mathrm{S} = \frac{S_\mathrm{I}}{\sigma^2} \int_{f_c-B/2}^{f_c+B/2} \mathrm{d}f\, \mathbf{g}(\varphi; f)\mathbf{g}^\dagger(\varphi; f). \tag{2.81}$$

The integral is evaluated element-wise, as

$$\begin{aligned} [\mathbf{\Sigma}_\mathrm{S}]_{m,n} &= \frac{S_\mathrm{I}}{\sigma^2} \int_{f_c-B/2}^{f_c+B/2} \mathrm{d}f\, [\mathbf{g}]_m(\varphi_\mathrm{I}; f)[\mathbf{g}]_n^*(\varphi_\mathrm{I}; f) \\ &= \frac{S_\mathrm{I}}{\sigma^2} \operatorname{sinc}\left[\pi B \gamma_{mn}(\varphi_\mathrm{I})\right] \exp\left[2\pi \mathrm{i} f_c \gamma_{mn}(\varphi_\mathrm{I})\right], \end{aligned} \tag{2.82}$$

where

$$\gamma_{mn}(\varphi_\mathrm{I}) = \frac{d}{c}(m-n)\sin\varphi_\mathrm{I}. \tag{2.83}$$

The finite bandwidth of the interference causes the signal to decorrelate over the array, as seen by the sinc-function. The spatial covariance matrix can be expanded in the eigenbasis as

$$\mathbf{\Sigma}_\mathrm{S} = \sum_{l=0}^{L-1} \lambda_l \mathbf{s}_l \mathbf{s}_l^\dagger \tag{2.84}$$

with orthogonal eigenvectors $\mathbf{s}_l$ and associated eigenvalues $\lambda_l$. Each eigenvector can be understood to represent an independent narrowband interference with power equal to its eigenvalue. Thus, one wideband source of interference is equivalent to several independent narrowband interfering signals from different directions,

where the effective number of the decomposition corresponds the the number of eigenvalues that exceed the system noise, *i.e.*, $|\{\lambda_l > 1 : l = 0, 1, \ldots, L-1\}|$. This "interference rank" depends non-trivially on the interference power, the angle-of-arrival, and the spectral density [86]. Importantly, if the wideband effects are sufficiently severe, and the interference rank exceeds the number of degrees of freedom in the array, the adaptive beamforming will not be able to suppress it.

Chapter 3

# Quantum Metrology

## 3.1 Towards quantum radar

In this chapter, our goal is to understand how quantum effects can be incorporated in radar operation, what the implications are, and whether there are advantages to be had by exploiting such effects. At first glance, such an analysis should follow similar steps as those in Chapter 2, modelling a system that is able to transmit and receive electromagnetic waves and measuring whether the received signal contains reflections off of targets. However, we will follow the established literature on quantum radar and use a simplified modelling scheme that is, at best, radar-like. The main addition in leaving the purely classical description is that the electromagnetic field is described by quantum mechanics. The toolbox used to analyse radar-like problems with quantum effects produces results that are less precise than those in Chapter 2, relying more on asymptotic relations and bounds. Nevertheless, this text strives to maintain some theoretical coherence between classical and quantum radar as there are many similarities. Throughout this chapter we use natural units. That is, we have $\hbar = 1$ for the reduced Planck constant and $c = 1$ for the speed of light, unless stated otherwise.

## 3.2 Notation in quantum mechanics

In simple terms, quantum mechanics is the framework that governs physical dynamics at small scales, such as for atoms and molecules. In quantum mechanics, the quantities are described in terms of states – denoted by kets $|\psi\rangle$ with the dual bras $\langle\psi|$ – and operators – denoted with hats $\hat{x}$. Expectation values for quantum states are written with the 'bra-ket' notation $\langle\hat{O}\rangle = \langle\psi|\,\hat{O}\,|\psi\rangle$, where $\hat{O}$ is the Hermitian operator of some observable. Our focus will mainly be on *mixed* states, which describe statistical ensembles of quantum states. Mixed states are denoted

by the density operator[1]

$$\rho = \sum_{k=0}^{K-1} p_k \left|\psi_k\right\rangle\left\langle\psi_k\right|, \tag{3.1}$$

with non-zero weights $p_k$ such that $\operatorname{tr}\rho = 1$. The density operator satisfies $\operatorname{rank}[\rho] \leq K$, with equality if all $|\psi_k\rangle$ are linearly independent. If $\operatorname{rank}[\rho] = 1$, the state is said to be 'pure' and may be written simply as the corresponding ket. All the dynamics of a quantum mechanical system is described by the time evolution of the density operator.

In any quantum mechanical experiment we should be interested in the outcome of the measurement result. Such results may be statistical in nature, either because the quantum system itself produces a random outcome, or because the measurement setup is subject to fluctuations and noise. The 'Born rule' is an axiom of quantum mechanics that tells us how to get classical statistics out of the density operator which done through a description of how the system is measured. Without going into details, a 'measurement' that gives rise to an observation $X \in \Omega_X$ is described by the operator[2] $\hat{\Pi}_X$. A classical probability distribution is generated from the quantum state as $\Pr_X(x) = \operatorname{tr}\hat{\Pi}_X\rho$. For this to make sense the sum of all measurement operators must resolve the identity, $\sum_{X\in\Omega_X}\hat{\Pi}_X = \hat{\mathbb{I}}$, which is simply a statement of conservation of probability. Importantly, one can imagine the task of an optimised experimental setup implementing a particular set of measurement operators to realise certain properties of the resulting probability distribution. We will return to this concept.

## 3.3 Quantising the electromagnetic field

Now, we sketch in an informal manner how electromagnetics can be made compatible with quantum mechanics. The steps follow how the material is presented in textbooks on quantum optics, *e.g.*, Refs. [87, 88]. For a more rigorous derivation, see, *e.g.*, Ref. [89]. Our present goal is to promote the electric field $\vec{E}$ to a Hermitian quantum operator $\hat{E}$.

### 3.3.1 Classical electromagnetics

Our starting point is Maxwell's equations in terms of the scalar potential $\phi = \phi(\mathbf{R}, t)$ and the vector potential $\vec{A} = \vec{A}(\mathbf{R}, t)$, at position $\mathbf{R}$ and time $t$. The free-space electric field is determined by $\vec{E} = -\nabla\phi - \partial_t\vec{A}$ and the magnetic field is determined by $\vec{B} = \nabla\times\vec{A}$. Then, the Maxwell equations for the potentials are

$$\nabla^2\phi + \nabla\cdot\partial_t\vec{A} = -\vec{\sigma}, \tag{3.2}$$

$$\nabla(\nabla\cdot\vec{A}) - \nabla^2\vec{A} + \partial_t\nabla\phi + \partial_t^2\vec{A} = \vec{J}, \tag{3.3}$$

[1] By tradition, the density operator alone does not wear the operator hat.
[2] Most generally, a positive operator-valued measure (POVM).

where $\vec{\sigma}$ and $\vec{J}$ is the charge and current density, respectively. Now separate the current density into transverse and longitudinal components, $\vec{J} = \vec{J}_{\mathrm{T}} + \vec{J}_{\mathrm{L}}$, with $\nabla \cdot \vec{J}_{\mathrm{T}} = 0$ and $\nabla \times \vec{J}_{\mathrm{L}} = 0$. In the Coulomb gauge, with $\nabla \cdot \vec{A} = 0$, the Maxwell equations are

$$\nabla^2 \phi = -\vec{\sigma}, \tag{3.4}$$

$$\partial_t \nabla \phi = \vec{J}_{\mathrm{L}}, \tag{3.5}$$

$$-\nabla^2 \vec{A} + \partial_t^2 \vec{A} = \vec{J}_{\mathrm{T}}. \tag{3.6}$$

Thus, we have decoupled the electrostatics determined by $\vec{\sigma}$ and $\vec{J}_{\mathrm{L}}$ from the electromagnetic waves determined by $\vec{J}_{\mathrm{T}}$.

Now, we continue with the transverse Eq. (3.6) alone, and consider the free field where $\vec{J}_{\mathrm{T}} = 0$. This results in the homogeneous wave equation

$$-\nabla^2 \vec{A} + \partial_t^2 \vec{A} = 0. \tag{3.7}$$

We impose periodic boundary conditions of a 'big box' with side length $L$, which require that the wavevectors must satisfy $\mathbf{k} = \frac{2\pi}{L}(n_x, n_y, n_z)^\top$, with $n_x, n_y, n_z \in \mathbb{Z}$. Now, expand the vector potential at position $\mathbf{R}$ and time $t$ in basis modes $\vec{b}_{\mathbf{k}\boldsymbol{\pi}}$ labelled by wavevector $\mathbf{k}$ and polarization $\boldsymbol{\pi} = \pm 1$, as

$$\vec{A}(\mathbf{R}, t) = \sum_{\mathbf{k},\boldsymbol{\pi}} \vec{b}_{\mathbf{k}\boldsymbol{\pi}} \left[ a_{\mathbf{k}\boldsymbol{\pi}}(t) \mathrm{e}^{\mathrm{i}\mathbf{k}\cdot\mathbf{R}} + a^*_{\mathbf{k}\boldsymbol{\pi}}(t) \mathrm{e}^{-\mathrm{i}\mathbf{k}\cdot\mathbf{R}} \right]. \tag{3.8}$$

By treating each mode in Eq. (3.7) separately, we have for mode $\mathbf{k}\boldsymbol{\pi}$ the harmonic oscillator equations

$$\partial_t^2 a_{\mathbf{k}\boldsymbol{\pi}}(t) + \omega_k^2 a_{\mathbf{k}\boldsymbol{\pi}}(t) = 0, \tag{3.9}$$

with frequency $\omega_k = |\mathbf{k}|$, for each field amplitude. The quantised frequencies are strictly a consequence of the periodic boundary conditions and are purely classical. The central step of quantising the field is to impose the quantum harmonic oscillator to Eq. (3.9) and to promote the mode amplitudes to operators.

### 3.3.2 The harmonic oscillator

The harmonic oscillator is the linear theory of oscillation. As a quick orientation, we quickly look at the classical harmonic oscillator. Assume a particle with mass $m$ is affected by forces linear in generalized displacement $q$ with some spring constant $\kappa$. The Hamiltonian of this classical harmonic oscillator is

$$H = \frac{p^2}{2m} + \frac{\kappa q^2}{2}, \tag{3.10}$$

where the canonical conjugate momentum is $p = m\dot{q}$. Applying the Hamilton equations of motion [90], $\dot{q} = \partial_p H$ and $\dot{p} = -\partial_q H$ gives the equation of motion as $\ddot{q} + \omega^2 q = 0$, where $\omega^2 = \kappa/m$. The general solution for $q$ is

$$q(t) = c_- \mathrm{e}^{-\mathrm{i}\omega t} + c_+ \mathrm{e}^{\mathrm{i}\omega t}, \tag{3.11}$$

where the constants $c_+, c_- \in \mathbb{C}$ are determined by initial conditions. This solution describes harmonic periodic motion with the radial frequency $\omega$.

The *quantum* harmonic oscillator can be introduced with the Hamiltonian operator

$$\hat{H} = \frac{1}{2}\left(\hat{q}^2 + \hat{p}^2\right), \tag{3.12}$$

where $\hat{q}$ and $\hat{p}$ are now Hermitian quantum operators in suitable units. Promoted to operators, the position and momentum satisfy the commutation relation $[\hat{q}, \hat{p}] = \hat{\mathbb{I}}\mathrm{i}$. The non-commuting nature of these conjugate operators implies that the respective variances jointly satisfy the Heisenberg uncertainty relation

$$(\Delta q)^2 (\Delta p)^2 \geq \frac{1}{4}. \tag{3.13}$$

The quantum harmonic oscillator algebra is given with the Bosonic annihilation and creation operators $\hat{a}$ and $\hat{a}^\dagger$, satisfying the commutation relation $[\hat{a}, \hat{a}^\dagger] = \hat{\mathbb{I}}$. The quantum harmonic oscillator is naturally represented in a Fock space with kets $|n\rangle$, where the index $n = 0, 1, 2, \ldots$ labels the occupation number. The operators $\hat{a}$ and $\hat{a}^\dagger$ are also referred to as ladder operators, for their action on $|n\rangle$, as $\hat{a}\,|n\rangle = \sqrt{n}\,|n-1\rangle$ and $\hat{a}^\dagger\,|n\rangle = \sqrt{n+1}\,|n+1\rangle$, 'stepping' up and down between states with different occupation numbers. This invites the use of the *number operator* $\hat{N} = \hat{a}^\dagger\hat{a}$, for which $|n\rangle$ is an eigenstate: $\hat{N}\,|n\rangle = n\,|n\rangle$. The ladder operators are related to the position and momentum operators of the oscillator by the relations

$$\hat{q} = \frac{1}{\sqrt{2}}\left[\hat{a}^\dagger + \hat{a}\right], \tag{3.14}$$

$$\hat{p} = \frac{\mathrm{i}}{\sqrt{2}}\left[\hat{a}^\dagger - \hat{a}\right]. \tag{3.15}$$

Rewriting the Hamiltonian operator of Eq. (3.12) in terms of the ladder operators and simplifying yields

$$\hat{H} = \hat{N} + \frac{1}{2}. \tag{3.16}$$

That is, for the Fock state $|n\rangle$, the expectation value of the Hamiltonian reads $\langle\hat{H}\rangle = n + \frac{1}{2}$. This additional term of $\frac{1}{2}$ tells us that even the state with occupation number zero has finite energy. This special minimum energy state, the vacuum $|0\rangle$, exhibits fluctuations.

### 3.3.3 Quantised electromagnetics

Now that we are familiar with the harmonic oscillator, we can go back to Eq. (3.9) and take the solution $a_{\mathbf{k}\boldsymbol{\pi}}(t) = a_{\mathbf{k}\boldsymbol{\pi}}\mathrm{e}^{-\mathrm{i}\omega_k t}$, similarly to Eq. (3.11). The field coefficient $a_{\mathbf{k}\boldsymbol{\pi}}$ is now promoted to a quantum operator, as $a_{\mathbf{k}\boldsymbol{\pi}} \to \hat{a}_{\mathbf{k}\boldsymbol{\pi}}$, where $\hat{a}_{\mathbf{k}\boldsymbol{\pi}}$ takes the role of a Bosonic annihilation operator. The occupation number $n$ of the Fock state $|n\rangle$ refers to the number of *photons* of that mode. Now, we introduce a new

phase $\varphi = \omega t + \mathbf{k} \cdot \mathbf{R}$ and again drop the subscript $\mathbf{k\pi}$. Then, as an operator, the electric field is

$$\hat{E}(\varphi) = \frac{E_\omega}{\sqrt{2}} \left( \hat{a} \mathrm{e}^{-\mathrm{i}\varphi} + \hat{a}^\dagger \mathrm{e}^{\mathrm{i}\varphi} \right) \tag{3.17}$$

where $E_\omega$ is the electric field amplitude of one photon with frequency $\omega$. If the field is measured in units of $E_\omega = 1$, all relations are simplified. Rewriting the electric field operator in terms of the generalized position and momentum with the relations of Eq. (3.14) and Eq. (3.15) yields

$$\hat{E}(\varphi) = \hat{q} \cos \varphi + \hat{p} \sin \varphi. \tag{3.18}$$

That is, the operators $\hat{q}$ and $\hat{p}$ take the role of *quadratures*. We take $\hat{q}$ to be the in-phase component and $\hat{p}$ to be the orthogonal component, and refer them jointly as the quadrature operators.

### 3.3.4 Multimode light

Even though we omit the explicit operator subscript that labels the wavenumber and polarization, it is nevertheless important to introduce a joint notation for states that consist of several modes, *e.g.*, $|n_1\rangle \otimes |n_2\rangle \otimes \ldots \otimes |n_N\rangle$. Analysis of multimode-states can be made more convenient by collecting the quadrature operators for each mode in the vector[3]

$$\hat{\mathbf{r}} = \begin{bmatrix} \hat{q}_1 & \hat{p}_1 & \hat{q}_2 & \hat{p}_2 & \ldots & \hat{q}_N & \hat{p}_N \end{bmatrix}^\top. \tag{3.19}$$

Between different modes, the quadrature operators commute. The multimode commutation relation reads $[[\hat{\mathbf{r}}]_i, [\hat{\mathbf{r}}]_j] = \mathrm{i}\, [\mathbf{\Omega}]_{i,j}$. Here $\mathbf{\Omega} = \mathbb{I}_N \otimes \left[\begin{smallmatrix} 0 & 1 \\ -1 & 0 \end{smallmatrix}\right]$ is the *symplectic form*.

The quantisation can be extended to the continuum by taking the limit of an infinite size big box: $L \to \infty$. In this limit, the Bosonic operators are labelled by the continuous frequency $\omega$, as $\hat{a}_k \to \hat{a}(\omega)$. Then it makes sense to introduce time domain operators as Fourier transforms of frequency space operators

$$\hat{a}(t) = \frac{1}{\sqrt{2\pi}} \int_{-\infty}^{\infty} \mathrm{d}\omega\, \mathrm{e}^{\mathrm{i}\omega t} \hat{a}(\omega). \tag{3.20}$$

For some applications, such as light pulses, it is useful to use the formalism with photon-wavepacket operators

$$\hat{a}_\xi = \int_{-\infty}^{\infty} \mathrm{d}t\, \xi(t) \hat{a}(t) \tag{3.21}$$

for a pulse shape $\xi(t)$. If we consider an orthonormal set of pulses[4] $\{\xi_i(t)\}_{i=1,2,\ldots}$, we retain the Bosonic commutation relation as $\left[\hat{a}_{\xi_i}, \hat{a}^\dagger_{\xi_j}\right] = \hat{\mathbb{I}} \delta_{i,j}$. When discussing

[3] Another common ordering is $\hat{\mathbf{s}} = [\hat{q}_1\, \hat{q}_2\, \ldots\, \hat{q}_N\, \hat{p}_1\, \ldots\, \hat{p}_N]^\top$. For this convention the symplectic form is $\mathbf{\Omega} = \left[\begin{smallmatrix} 0 & 1 \\ -1 & 0 \end{smallmatrix}\right] \otimes \mathbb{I}_N$.

[4] A set of pulse shapes that satisfy $\int_{-\infty}^{\infty} \mathrm{d}t\, \xi_i(t) \xi_j^*(t) = \delta_{i,j}$ for all $i$ and $j$.

radar-like applications, these are the types of modes that are understood to be used, even though a simplified notation is maintained.

## 3.4 Gaussian quantum states

Gaussian states belong to a particular set quantum mechanical states that finds large use in quantum optics. For one, the large amount of mathematical structure exhibited by a Gaussian state allows for analytical treatment of many experimentally relevant problems. Many Gaussian states may also be readily prepared experimentally. There are many areas of applications for Gaussian states, beyond the scope of this thesis, see, *e.g.*, Ref. [91]. The theory presented here is primarily based on the review of Adesso *et al.* [92] and the book of Serafini [93].

Similarly to random variables distributed according to the multivariate normal distribution, the Gaussian states are completely characterised by the mean $\boldsymbol{\mu}$ and covariance matrix $\boldsymbol{\Sigma}$ of the quadratures. The mean vector has elements

$$[\boldsymbol{\mu}]_i = \langle [\hat{\mathbf{r}}]_i \rangle \tag{3.22}$$

and the covariance matrix has elements

$$[\boldsymbol{\Sigma}]_{k,l} = \frac{1}{2} \langle \{ [\hat{\mathbf{r}}]_k, [\hat{\mathbf{r}}]_l \} \rangle - [\boldsymbol{\mu}]_k [\boldsymbol{\mu}]_l. \tag{3.23}$$

This definition of the covariance matrix reduces to the classical one if the operators commute, but it differs from the one in Ref. [93] where the scaled covariance matrix $\boldsymbol{\sigma} = 2\boldsymbol{\Sigma}$ is used.

In addition to to being Hermitian and positive semi-definite, the non-commuting property of conjugate quadrature operators requires that covariance matrix satisfies

$$\boldsymbol{\Sigma} + \mathrm{i}\boldsymbol{\Omega}/2 \succeq 0, \tag{3.24}$$

where $\boldsymbol{\Omega}$ is the symplectic form. This is known as the Robertson-Schrödinger uncertainty relation.

### 3.4.1 Single-mode states

The *single*-mode Gaussian states can be parametrized in terms of a $2 \times 1$ mean vector and a $2 \times 2$ covariance matrix. In this section, we present some particular states before presenting the canonical generic Gaussian single-mode state. Here, without loss of any generality, we use a reference phase such that the covariance matrix is diagonal. The minimum energy *vacuum* state $|0\rangle$ has zero mean and diagonal covariance matrix with the variance $\frac{1}{2}$. In fact, the vacuum is a *minimum variance* state. That is, the state containing zero photons has a minimum variance of $\frac{1}{2}$ for both quadratures. If a state can achieve a measurement variance smaller than $\frac{1}{2}$, it can be said to exhibit quantum advantage.

### Coherent State

If we start the vacuum state and displace the mean to some non-zero vector, we find the *coherent state*, which is the eigenstate of the annihilation operator. That is, the coherent state $|\alpha\rangle$, labelled by the parameter $\alpha \in \mathbb{C}$, satisfies $\hat{a}\,|\alpha\rangle = \alpha\,|\alpha\rangle$. The coherent state parameter can be written in polar form $\alpha = \sqrt{N_{\text{coh}}}\mathrm{e}^{\mathrm{i}\phi}$ for a phase $\phi \in [0, 2\pi)$ and average number of photons $N_{\text{coh}} = \langle\alpha|\hat{N}|\alpha\rangle$. The statistical moments are the mean

$$\boldsymbol{\mu} = \sqrt{2}\begin{bmatrix}\mathfrak{Re}\,(\alpha)\\ \mathfrak{Im}\,(\alpha)\end{bmatrix} \tag{3.25}$$

and covariance matrix

$$\boldsymbol{\Sigma} = \frac{1}{2}\begin{bmatrix}1 & 0\\ 0 & 1\end{bmatrix}. \tag{3.26}$$

In some sense, the coherent state behaves as a classical state, describing the state produced by a monochromatic laser. It is also a minimum variance state. For this reason it often serves as the classical benchmark to beat in a quantum enhanced protocol.

### Single-mode squeezed vacuum

For the coherent state and the vacuum state, the variance is symmetrically shared between the two quadratures. However, states can be prepared where this uncertainty is asymmetrically distributed. The possibly simplest example of such a state is the *squeezed* vacuum state, where the variance in one quadrature is reduced, while the orthogonal quadrature sees an increase in variance. In the covariance matrix, this can be parametrised as

$$\boldsymbol{\Sigma} = \frac{1}{2}\begin{bmatrix}s & 0\\ 0 & s^{-1}\end{bmatrix}, \tag{3.27}$$

with the squeezing parameter $s \in (0, \infty)$. Squeezing is an active process, adding $N_{\text{sq}} = \frac{1}{4}\left(s + s^{-1}\right) - \frac{1}{2}$ average photons to the vacuum.

### Thermal state

So far, we have considered pure states. We will need also the mixed thermal state with density matrix

$$\rho_{\text{th}} = \frac{1}{N_{\text{th}}+1}\sum_{n=0}^{\infty}\left(\frac{N_{\text{th}}}{N_{\text{th}}+1}\right)^{n}|n\rangle\langle n|\,, \tag{3.28}$$

which is a Gaussian state that is characterised by zero mean and covariance matrix

$$\boldsymbol{\Sigma} = \begin{bmatrix}N_{\text{th}}+\frac{1}{2} & 0\\ 0 & N_{\text{th}}+\frac{1}{2}\end{bmatrix}. \tag{3.29}$$

This state models the thermal equilibrium state at temperature $T$, where the average number of photons $N_{\text{th}}$ is given by the Bose-Einstein distribution at zero chemical potential

$$N_{\text{th}} = \left(\mathrm{e}^{hf/k_{\text{B}}T} - 1\right)^{-1}, \tag{3.30}$$

where $f$ is the frequency, $h$ is the Planck constant and $k_{\text{B}}$ the Boltzmann constant. As an example, for a system operating with microwave frequencies at room temperature the thermal background is strong, with $N_{\text{th}} \simeq 1000$, while for visible light $N_{\text{th}} \simeq 0$. To have negligible thermal background at microwave frequencies, the ambient temperature has to be reduced to a few milliKelvin, and this can be achieved with dilution refrigerators.

#### Displaced squeezed thermal state

Finally, the generic single-mode Gaussian state can be generated by squeezing a thermal state with $N_{\text{th}}$ number of photons and displacing the mean [94]. That is, the canonical Gaussian single-mode state is characterised by the mean

$$\boldsymbol{\mu} = \begin{bmatrix} \bar{q} \\ \bar{p} \end{bmatrix} \tag{3.31}$$

and the covariance matrix

$$\boldsymbol{\Sigma} = \begin{bmatrix} \left(N_{\text{th}} + \frac{1}{2}\right) s & 0 \\ 0 & \left(N_{\text{th}} + \frac{1}{2}\right) s^{-1} \end{bmatrix}, \tag{3.32}$$

where $s \in (0, \infty)$ is again the squeezing and $\bar{q}, \bar{p} \in \mathbb{R}$ are the displacements. The total number of photons in this generic state is $N = N_{\text{coh}} + N_{\text{sq.th}} + N_{\text{th}}\left(2N_{\text{sq.th}} + 1\right)$. As can be seen, increasing the mean adds 'coherent' photons linearly, while the squeezing or changing the temperature of the thermal state adds photons non-linearly, with $N_{\text{sq.th}} = \frac{2N_{\text{th}}+1}{4}\left(s + s^{-1}\right) - \frac{1}{2}$.

### 3.4.2 Two-mode states

With two modes, the mean vector is now of size $4 \times 1$ and the covariance matrix is of size $4 \times 4$. This means that a generic two-mode Gaussian system has 14 free parameters. The appended **Paper VII** considers various symmetries and constraints to reduce the number of free parameters for a certain type of problem. Here, we neglect to state explicitly the fully generic two-mode state, and describe instead two special two-mode states in some detail.

#### Two-mode squeezed vacuum

An important non-classical feature that is introduced with two-mode states is that we can have *entanglement* between the modes. A state that exhibits entanglement

is the two-mode squeezed vacuum state (TMSV). It is, in fact, the *maximally* entangled two-mode state on a per-photon basis [91].

The TMSV state can be generated with parametric amplification of the vacuum, generating pairs of photons in two entangled modes. The entangled modes are often referred to as *signal* and *idler*, respectively. If the two modes are separated, and the signal is used as probe in a metrological protocol, one can achieve entanglement-enhanced performance, which may surpass that of a purely classical probe. Because the TMSV state is populated by pairwise photons, the average number of photons $N_S$ in the signal and idler are equal. The TMSV state has few degrees of freedom, with zero mean and a covariance matrix

$$\mathbf{\Sigma}_{\text{TMSV}} = \begin{bmatrix} N_S + 1/2 & 0 & \sqrt{N_S(N_S+1)} & 0 \\ 0 & N_S + 1/2 & 0 & -\sqrt{N_S(N_S+1)} \\ \sqrt{N_S(N_S+1)} & 0 & N_S + 1/2 & 0 \\ 0 & -\sqrt{N_S(N_S+1)} & 0 & N_S + 1/2 \end{bmatrix}. \tag{3.33}$$

The statistics of each mode individually is indistinguishable from thermal noise, but the inter-mode covariance proportional to $\sqrt{N_S(N_S+1)}$ – being larger than the classical limit of $N_S$ – reveals that the state exhibits non-classical correlations. These non-classical correlations are apparent in the regime with few photons per mode, $N_S \ll 1$, where $\sqrt{N_S(N_S+1)} \gg N_S$. In the strong signal regime, with $N_S \gg 1$, the non-classical correlations are basically indistinguishable from the classical correlations as $\sqrt{N_S(N_S+1)} \simeq N_S$.

### Correlated thermal noise

As a classical counterpart to the TMSV state, we study the two-mode state consisting of correlated thermal modes. We denote this state as classically correlated noise (CCN). To our knowledge, this state has not been widely studied in literature, which merits its inclusion. The CCN state is generated by mixing the noise from two independent thermal sources at temperatures $T_H$ and $T_C$, described by the operators $\hat{a}_H$ and $\hat{a}_C$. Here, the subscripts $H$ and $C$ refer to 'hot' and 'cold', respectively, indicating that we take $T_H \geq T_C$. Each thermal source is in the single-mode thermal state, with average number of thermal photons denoted by $N_H$ and $N_C$, respectively.

The CCN state is prepared by mixixing two thermal sources over a beamsplitter labelled by the variable reflection coefficient $\beta \in [0, 1]$. The output modes, designated as signal and idler to mirror the TMSV state, are

$$\hat{a}_S^{\text{CCN}} = \sqrt{\beta}\hat{a}_H + \sqrt{1-\beta}\hat{a}_C, \tag{3.34}$$

$$\hat{a}_I^{\text{CCN}} = -\sqrt{1-\beta}\hat{a}_H + \sqrt{\beta}\hat{a}_C. \tag{3.35}$$

Being a Gaussian state, the CCN state is characterised by having a zero first order

moment and the covariance matrix

$$\mathbf{\Sigma}_{\text{CCN}} = \begin{pmatrix} N_S + 1/2 & 0 & \gamma_{SI} & 0 \\ 0 & N_S + 1/2 & 0 & \gamma_{SI} \\ \gamma_{SI} & 0 & N_I + 1/2 & 0 \\ 0 & \gamma_{SI} & 0 & N_I + 1/2 \end{pmatrix}, \tag{3.36}$$

where $N_S = \beta N_C + (1-\beta) N_H$, $N_I = (1-\beta) N_C + \beta N_H$, and $\gamma_{SI} = \sqrt{\beta(1-\beta)}(N_H - N_C)$. As long as the input modes have different number of photons on average, corresponding to different temperature, the output modes $\hat{a}_S^{\text{CCN}}$ and $\hat{a}_I^{\text{CCN}}$ are correlated.

## 3.5 Interacting with a noisy environment

In modelling radar-like scenarios, quantum states will take the role of signals. In contrast to the noise radar treatment of Chapter 2, we do not have access to a digital reference copy of the signal. Instead of transforming a particular signal, the quantum transmit-to-receive channel acts as a mapping of the state. Formally, the channel can be seen as the time evolution of the probe state $\rho$ through the Lindblad equation [95, 96]. During the transmit-to-receive time, the state interacts with the target and environment through $K$ modes as

$$\dot{\rho} = \left[\hat{H}, \rho\right] + \sum_{k=0}^{K-1} \gamma_k \left( \hat{\Gamma}_k \rho \hat{\Gamma}_k^\dagger - \frac{1}{2} \left\{ \hat{\Gamma}_k^\dagger \hat{\Gamma}_k, \rho \right\} \right), \tag{3.37}$$

where $\gamma_k$ describes the coupling strength through the interaction of operator $\hat{\Gamma}_k$. To be accessible for analysis, the model will be relatively simple, with the following assumptions as delimitations.

- Only one target is modelled and the interaction occurs in an environment of thermal noise with a known $N_B$ number of photons on average. There are no other targets or clutter.
- The explicit time dependence is dropped with a fixed transmit-to-receive interaction time that is known.
- There is no Doppler shift induced on the state, *i.e.*, the target has zero relative velocity.
- The interaction is dissipative and described by the operators $\hat{\Gamma}_0 = \hat{a}$ and $\hat{\Gamma}_1 = \hat{a}^\dagger$ with coupling rates $\gamma_0 = \gamma(1 + N_B)$ and $\gamma_1 = \gamma N_B$, respectively.

In **Paper VII** we refer to the mapping corresponding to these dynamics as the *Lossy Bosonic channel*. This type of interaction has been studied for loss sensing [97–99].

As an alternative, the dynamics of the channel can be cast in the Heisenberg picture as a beamsplitter mixing the signal mode $\hat{a}$ and an environmental thermal

noise mode $\hat{b}$ with $N_B$ number of photons on average. For Gaussian states, this takes the form of the transformation

$$\hat{a} \to \eta\hat{a} + \sqrt{1-\eta^2}\,\hat{b}, \tag{3.38}$$

where the transmission coefficient is $\eta \equiv \eta(t) = \mathrm{e}^{-t\gamma/2}$. This formalism has been used to model the transmit-to-receive channel of radar-like scenarios, see, *e.g.*, Ref. [100]. For a two-mode state, partitioned into signal and idler, this channel can be cast as a map of the mean and covariance matrix as

$$\begin{pmatrix} \bar{q}_S \\ \bar{p}_S \\ \bar{q}_I \\ \bar{p}_I \end{pmatrix} \to \begin{pmatrix} \eta\bar{q}_S \\ \eta\bar{p}_S \\ \bar{q}_I \\ \bar{p}_I \end{pmatrix}, \tag{3.39}$$

$$\begin{pmatrix} \boldsymbol{\Sigma}_S & \boldsymbol{\Sigma}_{SI} \\ \boldsymbol{\Sigma}_{SI}^\dagger & \boldsymbol{\Sigma}_I \end{pmatrix} \to \begin{pmatrix} \eta^2\boldsymbol{\Sigma}_S + (1-\eta^2)\left(N_B + \frac{1}{2}\right)\mathbb{I} & \eta\boldsymbol{\Sigma}_{SI} \\ \eta\boldsymbol{\Sigma}_{SI}^\dagger & \boldsymbol{\Sigma}_I \end{pmatrix}. \tag{3.40}$$

It is common to introduce a normalisation of the background noise, as $N_B \to N_B/(1-\eta^2)$. The normalisation removes the effect where measuring a background gives information of $\eta$, regardless of the signal mode, referred to as the 'shadow effect' [101]. This is done *ad hoc* to eliminate any metrological power of the background and isolate the effect of the signal. Intuitively, the normalised channel models a scenario where the target, if present, emits an average number of thermal photons that equals that of the background environment were the target absent.

Quantum effects are typically relevant only for states with few photons and amplification may be necessary to enable measurement of the signals involved. The simplest possible model of amplification that is compatible with quantum mechanics [102] – a phase-insensitive amplifier transformation – can be written

$$\hat{a} \to \sqrt{G}\hat{a} + \sqrt{G-1}\hat{b}^\dagger, \tag{3.41}$$

where the amplifier power gain is $G \geq 1$.

## 3.6 Metrology

In general, metrology is the theory of measurement. Quantum mechanics sets the fundamental limits on how well any such method can be implemented for physical systems. While many quantitative fields can perform these inferences perfectly well without an in-depth understanding of quantum mechanics, there are fields where quantum features become relevant, see, *e.g.*, Refs. [4, 103] for reviews on quantum metrology.

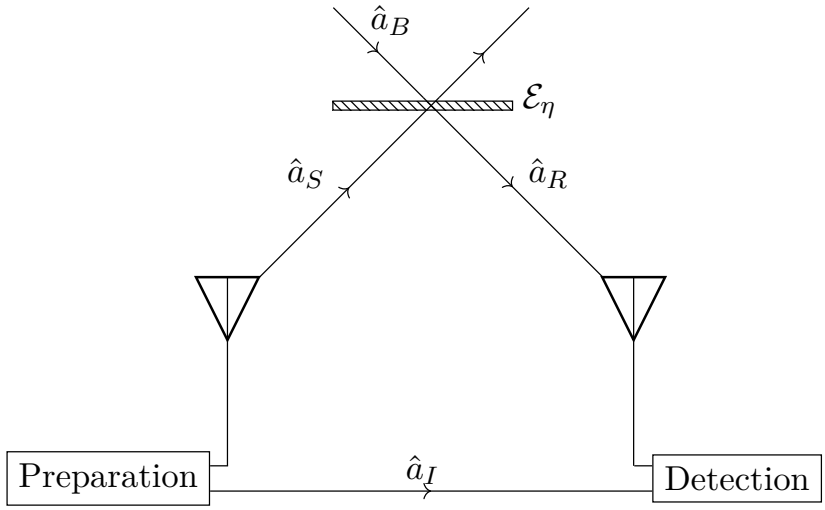


**Figure 3.1:** Schematic overview of the QI protocol. An entangled signal-idler pair is prepared. The signal mode $\hat{a}_S$ is sent to interact with an unknown channel $\mathcal{E}_\eta$, modelled according to Eq. (3.38). The return mode $\hat{a}_R$ is jointly measured with the retained idler $\hat{a}_I$. If the correlation is sufficiently strong, the detector declares in favour of target presence. [Reproduced from Figure 2 of **Paper V**.]

### 3.6.1 Quantum Illumination

As a subset of metrology, hypothesis testing forms the basis for most of quantitative science by systematically deciding which of a prescribed set of descriptions best fit observed data. As we have seen in Chapter 2, a binary hypothesis test also performs the central detection function in a radar system. Within the world of quantum detection theory we a focus on the QI protocol, since it serves as the recurring foundation of quantum radar. With the restrictions discussed in the transmit-to-receive model, quantum illumination by itself fails to perform some of the tasks of a conventional radar protocol, such as measuring distance. It can be argued that QI is at best radar-like.

Explicitly, QI discriminates between two possible states in the following way: A probe state consisting of an entangled signal-idler pair with $N_S$ number of photons on average is generated as a TMSV state. The signal is passed through one of two possible channels, where it is unknown which channel is actually in effect. Both channels are Bosonic lossy thermal noise channels injecting $N_B$ noise photons on average, see Section 3.5. The two channels are distinguished by different transmission coefficients $\eta$, here labelled by different hypotheses as

$$\begin{aligned} &\mathcal{H}_0 : \eta = 0 \\ &\mathcal{H}_1 : \eta = \eta_1 \quad \text{with } 0 < \eta_1 \ll 1. \end{aligned}$$

Both $\mathcal{H}_0$ and $\mathcal{H}_1$ are *simple* hypotheses, which is required for the tools used to be valid. Back at the receiver we get either the state $\rho_0$ or the state $\rho_1$, depending on which hypothesis is true, see Figure 3.1. Comparing to Figure 2.1, the radar-

like qualities of QI should be clear, as determining if $\eta$ is non-zero is similar to detecting the presence of a radar target.

This test can be repeated independently for $M$ modes, for example by frequency multiplexing, or by repetition over time. The final task is thus to discriminate between $\rho_0^{\otimes M}$ and $\rho_1^{\otimes M}$, and decide which channel was in effect during the measurement. Since a sufficiently strong signal will outperform any weaker signal, a constraint imposed on the problem is that the average number of photons in the signal mode $N_S$ is fixed.

QI was developed for a symmetric binary hypothesis test, where the priors are assumed equal. The protocol seeks to minimise the total error probability $P_{\mathrm{E}}$, see Eq. (2.41). Instead of studying an exact expression for $P_{\mathrm{E}}$, an asymptotic bound is used. The quantum Chernoff bound [104, 105] is the central result that enables this analysis. It says, informally, that, as the number of repeated trials $M$ grows, the total error probability will asymptotically enter a regime where it is bounded from above by an exponentially decaying function, as $P_{\mathrm{E}} \leq \frac{1}{2}\exp[-M\xi_{\mathrm{C}}]$, where

$$\xi_{\mathrm{C}} = -\log\left(\min_{0\leq s\leq 1} \mathrm{tr}\left[\rho_0^s \rho_1^{1-s}\right]\right) \tag{3.42}$$

is the quantum Chernoff coefficient that determines the decay rate. It is in this situation that we can identify the Chernoff coefficient as the *error exponent*. Computation of $\xi_{\mathrm{C}}$ can be difficult and a more simpler approach is found by relaxing the inequality and computing instead the less tight Bhattacharrya bound with coefficient $\xi_{\mathrm{B}} \leq \xi_{\mathrm{C}}$. The Bhattacharrya coefficient[5] $\xi_{\mathrm{B}}$ is found from Eq. (3.42) by neglecting the minimisation procedure and requiring instead $s = \frac{1}{2}$. It is in this context that Tan *et al.* [30] established that the Chernoff coefficient for a coherent state probe is $\xi_{\mathrm{C}}^{\mathrm{coh.}} = \frac{\eta_1 N_S}{4N_B}$ and the Bhattacharrya coefficient for a TMSV probe with an entangled idler is $\xi_{\mathrm{B}}^{\mathrm{TMSV}} = \frac{\eta_1 N_S}{N_B}$, *i.e.*, a factor of four advantage, or approximately 6 dB, in the regime where $N_S \ll 1$, $N_B \gg 1$ and $\eta_1 \ll 1$.

One might ask as to what extent the coherent state serves as a relevant classical benchmark. Maybe there are other classical states that perform better? The answer can be understood quite simply. Fundamentally, there are limits to how well the discrimination task can be performed for *any* probe state. Ref. [107] states that the coherent state saturates a fundamental limit in the noise-free regime. This can be understood as a no-go for any quantum advantage in the low-noise regime because no probe can do better than to match the coherent state performance. Conversely, for the noisy regime the TMSV saturates the limit.

The final aspect of a discrimination protocol is the description of a receiver structure that, ideally, realises the theoretical performance. That is, the measurement operator should be constructed. For example, the optimal strategy is not possible

[5] In the literature, one encounters the term of Bhattacharrya *distance* [106], favouring a geometrical interpretation. Here, we use instead *coefficient* to keep the terminology consistent.

with local measurements [108] and a joint measurement strategy between the return mode and the idler is required. The receiver structures described in Ref. [32] realise only a sub-optimal factor of two in the error exponent. A receiver structure that *does* achieve the full factor of four advantage is described in Ref. [33], although building a device according to this scheme is technologically unfeasible. However, the existence of an optimal scheme, albeit as a theoretical concept, is important for the understanding of the QI protocol. As a complement to working with asymptotic results and somewhat abstract tools, important work has also been done with the task of practical implementations and comparison with classical protocols, see Ref. [109].

An important feature of quantum illumination is that entangled state protocol presents a discrimination advantage over a non-entangled state, even though the entanglement itself does not survive through the channel. That is, the advantage should not be understood as a residual entanglement, but the interpretation is rather that the signal-idler correlations of the probe state are stronger than those of any possible separable state [30].

As noted in Chapter 2, conventional radar avoids introducing any assumptions about the prior probabilities of target presence. While the original development of the QI protocol was for symmetric priors, it has also been extended to the general case of unknown, possibly asymmetric priors, more in line with conventional radar operation [110, 111]. Equivalently to the detector function discussed in Chapter 2, the problem is approached by maximising the probability of detection while ensuring that the probability of false alarm is bounded by some prescribed rate $\varepsilon$. In this situation we can not rely on the Chernoff bound, but instead turn to the similar asymptotic result of Stein's Lemma [112, 113], which states that, for any $\varepsilon$, the probability of a missed detection is bounded as the number of repeated trials tends to infinity. Informally, we understand this mathematically as

$$1 - P_{\mathrm{D}} \leq \exp[-MD(\rho_1||\rho_0)], \tag{3.43}$$

where

$$D(\rho_1||\rho_0) = \operatorname{tr} \rho_1 \left(\ln \rho_1 - \ln \rho_0\right) \tag{3.44}$$

is the quantum relative entropy between the two possible output states. It has been shown that also in this scenario, the TMSV state is optimal [114], but the nature of the advantage is slightly more complicated than a single number, as it depends non-trivially on the scenario. In fact, as $N_S \to 0$, the advantage of a TMSV state probe over a coherent state grows without bound. This may appear to be incredibly useful at first glance. However, due to the fact that the *absolute* discrimination strength goes to zero in the same limit, it is simply a result of the relative entropy tending to zero faster for the coherent state than for the TMSV state.

As Stein's Lemma is asymptotic, it does not incorporate the choice of $\varepsilon$. Higher order asymptotic terms for the quantum Stein's Lemma have been developed

by Li [115] and used to analyse the transition to asymptotic behaviour of QI in Ref. [110]. If we stick with the informal mathematical description, the semi-asymptotic Stein's Lemma takes the form

$$1 - P_{\mathrm{D}} \leq \exp\left[-MD(\rho_1||\rho_0) - \sqrt{MV(\rho_1||\rho_0)}\Phi^{-1}(\varepsilon)\right], \tag{3.45}$$

where the number of repeated trials $M$ is large, but finite. Here,

$$V(\rho_1||\rho_0) = \operatorname{tr}\rho_1\left[\ln\rho_1 - \ln\rho_0 - D(\rho_1||\rho_0)\right]^2 \tag{3.46}$$

is the relative entropy *variance* and $\Phi^{-1}$ is the inverse standard normal distribution. Note that $\Phi^{-1}(\varepsilon) < 0$ for $\varepsilon < \frac{1}{2}$, which implies that a smaller relative entropy variance is beneficial to the discrimination strength.

### 3.6.2 Fisher Information

As an alternative to the discrete decision problem, one can study the problem of estimation, where the value of an unknown parameter is to be determined. As in Chapter 2, we wish to construct an estimator that performs this task. Since the estimator is a function of random data, it is itself a random variable. Therefore, it is important to characterise the statistics of the estimator in order to quantify its performance.

Central to the performance of any estimator is its variance and, preferably, it should be made as small as possible. However, one may inquire how small the variance could be for *any* estimator and define an a criterion of optimality if this minimum is saturated. The tool of this analysis is the Cramér-Rao lower bound (CRLB) [72]. For a classical estimation problem, the CRLB is a result given in terms of a random variable $X$ that is distributed according to the parametric probability density function $p_X(x;\theta)$. If we wish to estimate the value of $\theta$ based on $M$ independent observations of $X$, the CRLB tells us that the minimum achievable variance of *any* unbiased estimator $T_\theta$ of $\theta$ is given by

$$\operatorname{var} T_\theta \geq (MI_\theta)^{-1}, \tag{3.47}$$

where

$$I_\theta = \mathbb{E}_X[(\partial_\theta \log p_X(x;\theta))^2] \tag{3.48}$$

is the Fisher information (FI) of $\theta$ with respect to the random variable $X$. A large FI indicates that the unknown parameter can be estimated with small variance.

When moving from classical statistics to quantum mechanics, we need to account for different possible measurements, giving rise to different classical statistics. Let $\rho_\theta$ be a density operator that depends on the continuous parameter $\theta$. The *quantum* Fisher information (QFI) [3] of this state is the FI maximised over all possible sets of POVMs $\{\hat{\Pi}_X\}$, *i.e.*,

$$J(\rho_\theta) = \max_{\{\hat{\Pi}_X\}} I_\theta. \tag{3.49}$$

Thus, the QFI is manifestly the maximally achievable FI, when the optimal measurement is implemented. The QFI can be computed as $J(\rho_\theta) = \mathrm{tr}\left[\rho_\theta \hat{\mathcal{L}}_\theta^2\right]$, where $\hat{\mathcal{L}}_\theta$ is the symmetric logarithmic derivative (SLD), defined as the solution to the Lyapnov equation

$$2\partial_\theta \rho_\theta = \hat{\mathcal{L}}_\theta \rho_\theta + \rho_\theta \hat{\mathcal{L}}_\theta. \tag{3.50}$$

Given this definition of the QFI, the CRLB generalises to the quantum case in the obvious manner. Stated together with the classical version of Inequality (3.47), the quantum CRLB says that

$$\mathrm{var}\, T_\theta \geq (M I_\theta)^{-1} \geq (M J(\rho_\theta))^{-1}. \tag{3.51}$$

That is, the variance of any unbiased estimator is lower bounded by the reciprocal QFI. Thus, the quantum CRLB presents the ultimate limit of the precision of any estimation task. Importantly, the quantum Cramér-Rao lower bound is achievable – there exist a POVM such that the classical Fisher information equals the QFI. However, the optimal measurement may be difficult or even impossible to implement due to technological limitations.

Chapter 4

# Publications

## 4.1 Noise radar

**Papers I-IV** cover different topics of noise radar. In order of publication, they report on the development of an experimental bistatic noise radar system, from initial tests in **Paper I** to real-time operation with a spatially adaptive array in **Paper IV**. The experimental results in these papers are supported by implementation and verification of the various algorithms and processing techniques of Chapter 2. For these publications, the theory development has been a secondary objective as main focus has been on the technical implementation and the novelty centred on experimental results. In particular, the experimental demonstrations have been focused on testing the system and processing in challenging scenarios with strong, extended clutter. The system itself has been designed to be relatively cheap and mobile.

A common challenge in these four papers is that noisy waveforms and continuous transmission severely impact the range coverage of the radar system due to the correlation noise floor (CNF). For this reason, we argue that, at least for ground-based noise radar systems, the CNF will always be a large problem in a monostatic setup, even with an optimised configuration to reduce the coupling between the transmitter and receiver antennas. This is because there will generally be ground clutter signals several orders of magnitude stronger than targets of interest and the clutter sidelobes will mask the signals from most targets of interest. Increasing the processed time-bandwidth product will reduce the CNF, but also brings other challenges such as mismatch losses from range-cell migration of moving targets. As we show in these publications, the techniques discussed in Chapter 2 can be used to mitigate the CNF due to clutter in addition to reducing the losses due to target movement. However, the algorithms are computationally expensive and may exhibit diminishing returns with increased efforts, and one should not rely

solely on processing techniques.

The experimental noise radar system operates at the L-band at $f_c = 1.3$ GHz and the final version is able to compute digital coherent processing in real-time covering a time-bandwidth product of up to 77 dB. Most of the signal processing is done on the Vivace platform developed by Intermodulation Products. By relying on pseudo-noise to generate the signals, there is no need to communicate the signal from the transmitter to the receiver, as pre-sharing the random number seed is sufficient. A requirement for this to be possible is that the transmitter is sufficiently linear to not distort the signal as it is transmitted. The bistatic system does rely on a GNSS[1] signal to synchronise the transmitter and receiver. For all these publications, the experimental data were recorded with a DJI Matrice 600 uncrewed aerial vehicle (UAV) acting as coopering target.

### 4.1.1 Paper I

As this is our first publication on the topic of bistatic noise radar, a significant amount of the material is focused on presenting the system and technical solutions. Linearity of the transmitter is evaluated in terms of correlation losses. The viability of bistatic operation as a method to mitigate the CNF is demonstrated as the target UAV is detected with an improvement in the signal strength of over 20 dB with respect to the effective noise floor compared to a monostatic configuration. Additionally, a CLEAN-based clutter suppression algorithm was used to further reduce the impact of clutter and direct signal interference, adding another 20 dB improvement.

### 4.1.2 Paper II

This paper attempts to recover the mismatch losses by compensating for target movement, as detailed in Section 2.3. We verify experimentally the effect of the target signal spreading into several range and Doppler bins, with a continuous illumination time of 1 s and the target UAV moving at approximately 11.5 m/s along a straight line. With knowledge of the true radial velocity, the moving target compensation technique manages to recover up to 13.6 dB of the signal strength, when compared to the average signal strength with no compensation. In this context, we discuss the losses involved and argue that, even with this approximate method, the spacing of matched velocities can not be too large. Finally, we characterised the UAV target's coherence time. The UAV is an electromagnetically complex target, with six uncovered rotor blades and there is no reason to assume it will scatter the signals coherently for extremely long observation times. Nevertheless, we observe that coherent integration is possible for, at least, a few seconds.

[1] Global Navigation Satellite System

### 4.1.3 Paper III

The CLEAN-based method of **Paper I** was, as implemented, an *ad hoc* solution to unmodified CLEAN not performing particularly well. This paper originated as an attempt to put the clutter suppression algorithm in a theoretical framework and to quantify its performance. The principles of multisignal GLRT detection with maximum likelihood estimates of unknown parameters were used to guide algorithmic development. The two resulting clutter suppression algorithms take the overall form of OMP and ECA, respectively, and manage to suppress the CNF by over 30 dB, a significant improvement over the CLEAN-based algorithm of **Paper I**. With these algorithms, we verified that the clutter environment is sufficiently stable that it can be mapped for reuse in the ECA-based algorithm over several seconds at least, and possibly significantly longer.

### 4.1.4 Paper IV

This paper represents a significant step forward in the capabilities of the noise radar system. Now, it may process detections in real-time, even in a bistatic configuration. The receiver side has been updated with a 8-element ULA allowing for spatial measurement of target signals for azimuthal direction finding. We demonstrate detection of the UAV target at a bistatic distance of several kilometres. The adaptive receiver array allows us to form suppress the direct signal from the transmitter. When using only the information of spatial correlations over the array there is no distinction between our own signal and uncorrelated interference. Thus, the adaptive suppression can be used for direct signal self-interference. For suppression of the direct signal to be possible in this configuration, the instantaneous power from the transmitter must overcome the receiver system noise. To achieve this, we measured in a quasi-monostatic setup, with only tens of metres bistatic separation. The results demonstrate that the direct signal interference can be reduced. However, we noted in this setup that wideband effects became highly relevant and the adaptive suppression failed if the transmitter was too close to the receiver. A possible future endeavour would be to expand the adaptive processing to better handle wideband signals. This can be done with a space-time adaptive setup.

## 4.2 Quantum Metrology

**Papers V-VIII** study various radar-like scenarios with the tools presented in Chapter 3. These papers are all in the field of quantum metrology, with loss sensing derived from the quantum radar project as the principal research topic. While the setting and tools are different from conventional radar, **Paper I** and **Paper II** analyse quantum illumination as an enhanced radar protocol in relation to the, at the time, recent experiments of Refs. [43–45] and targets an audience that are not experts on quantum mechanics.

Formally, the analysis in these four papers is related to the measurement of an unknown transmission coefficient and the recurring question is whether a quantum state provides an advantage of the semi-classical coherent state per signal photon.

### 4.2.1 Paper V

The principal goal of this paper is to further the understanding of CCN state, see Section 3.4.2, and its metrological properties as a radar protocol probe compared to an entangled probe. The CCN state is designed to model the classical reference used in Ref. [43]. We quantify the benefit of stronger correlations by computing the asymptotic ROC assuming heterodyne detection of both modes. Our results show that heterodyne detection, even ideal, increases the variance sufficiently to suppress any correlation advantage of the entangled probe state, in agreement with Ref. [39].

The discrimination strength *before* detection is further analysed with the semi-asymptotic result of the Quantum Stein's Lemma, see Eq. (3.45), using the formulas for Gaussian states from Ref. [110]. The results show that the TMSV state can supply an unbounded advantage over the asymmetric CCN state in terms of error exponent in the limit of vanishing probe brightness. It must be emphasised that the total discrimination strength tends to zero in the same limit which challenges whether the advantage can be useful in a practical measurement. For the advantage to be relevant there must be an external criterion that requires the probe brightness to be low.

Finally, since the experiments that inspired this paper used amplifiers in their setup, we analyse the impact of ideal phase-invariant amplification at various points of the protocol. We compute a simple criterion that shows how amplification of the idler suppresses any chance of a quantum advantage. However, since the publication of this paper it has been shown [51] that a sub-optimal quantum advantage can be realised with heterodyne measurement of the signal return mode, if the idler is measured homodyne conditioned on the heterodyne result.

### 4.2.2 Paper VI

This paper was prepared for the specific purpose of bridging a perceived gap between radar engineers and quantum optics researchers with respect to quantum radar, targeting the former as audience. Central to the analysis is the restrictions imposed by the regime in which QI exhibits its advantage, *i.e.*, where the signal photons are few per mode and the thermal background is bright. Outside of this regime there is no quantum advantage on offer and one may as well use a coherent state probe. Intuitively, transmitting a weak signal to find a target in a bright background will be difficult. In fact, it can be argued to be extremely difficult in a conventional radar context. For a typical radar scenario, covering distances of tens of kilometres, the transmit-to-receive ratio of power can be as small as $10^{-15}$ or even smaller. One must coherently detect many modes to be able to detect targets in this situation, which requires processing of a large time-bandwidth product. By restricting the system to operate in the regime with a quantum advantage, there is a discrepancy of at least ten orders of magnitude between what is technically realistic and what is required to approach the performance of conventional radar. Based on this analysis, we argue that the radar advantage offered by QI is so situational and technically complicated that it is difficult to even imagine an operational scenario where its implementation would provide a crucial benefit.

### 4.2.3 Paper VII

In this paper, we move on to quantum *estimation* where the task is to measure the value of the transmission coefficient. Our tools of this study are the QFI and the quantum CLRB. We investigate which input state, restricted to a certain power, maximises the QFI of the channel transmission coefficient.

Our work in this paper consists of a full characterisation of the optimal *Gaussian* probe state in single- and two-mode configuration. Even though this is a single-parameter estimation problem there are several degrees of freedom in the generic Gaussian state. The single-mode optimal state depends non-trivially on the average number of signal photons, the average number of thermal background photons and the true value of the transmission coefficient. To enable analytical results, it is crucial to establish canonical forms of the probe states with reduced degrees of freedom. The more involved analytical results were calculated with support from computer algebra software.

Additionally, we study the variant of the channel where the number of background photons is normalised to be independent of the transmission coefficient, known as the "no passive signature assumption" [4]. For this channel, with access to an entangled idler, we show that the TMSV state is globally optimal. We prove this result by showing that the QFI for the TMSV state saturates the fundamental upper bound proved in Ref. [107]. The result that the TMSV state is universally optimal when the shadow effect is removed was first reported without proof at the

2021 International Symposium on Information Theory [116]. After our publication of **Paper VII**, a longer version of Ref. [116] was published as Ref. [117].

### 4.2.4 Paper VIII

This paper is a manuscript that expands the dynamical interaction to include quadratic term, modelling two-photon absorption [118–120]. Overall, the toolbox is similar to the one of **Paper VII**, using the QFI to quantify performance of various quantum mechanical probe states. In contrast to **Paper VII**, we include non-Gaussian probe states in the analysis. The states we consider can be generated by a qubic interaction Hamiltonian and are referred to as 'tri-squeezed' because the generation process can be understood as three-mode down-conversion. Two-photon interaction and states generated from a qubic Hamiltonian are not easy to analyse with analytics and requires us to turn to numerics to compute the QFI. The results show that the QFI of two-photon absorption can be larger for the tri-squeezed probe states considered, particularly in the regime of few signal photons per mode. At the time of writing some work remains for this paper. In particular, the manuscript is missing a few results on the *realised* classical FI under certain common measurements, such as homodyne.

Chapter 5

# Conclusion and Outlook

At the start of this research project the goal was to investigate, and hopefully demonstrate experimentally, the technological feasibility of quantum radar. Being a project connected to Saab and the radar industry, it was unavoidable that the practical usefulness of quantum radar was incorporated in the investigations.

Communication between academia and industry and the relationship between pure research and technology development has been important. Regardless of the research field, it is a challenge to balance the presentation of results between technical correctness and ease of access. Overall, the philosophy around this has been to give special emphasis to presenting results in a relevant context with, if possible, an application in mind. The field of quantum radar, and the technology hype that proliferated about it at the time, was prone to misunderstandings by the radar engineering community about the nature and regime of the oft-cited quantum advantage over classical radar. With time, our understanding of the limitations of quantum radar grew and the experimental side of the project was diverted into classical[1] noise radar. This may appear as a drastic change, but occurred as a natural evolution. After the publication of **Paper V** and **Paper VI** we felt confident in our conclusions that practical applications of quantum radar for conventional settings were unfeasible. We appear to not be alone in this conclusion as it was noted in a recent pre-print [121] that the number of quantum radar publications published with the IEEE peaked around the years 2020 and 2021, with a sharp drop since. Time will tell if this is a permanent loss of interest or a just temporary dip in the hype cycle.

Since the protocol of quantum illumination involves the correlation between a noisy signal with a retained reference it can be understood as a type of noise radar. Even though radar may be considered a mature and established field of

[1] Classical as in non-quantum.

technology, there are still many interesting research challenges to tackle. Currently, the field of radar shifts more and more to digital solutions, which enables entirely new possibilities in signal and data processing. These developments may push radar using noise and other arbitrary waveforms into viable radar systems, where the correlation noise floor does not fundamentally restrict the space of applications. With our work in noise radar, documented in **Papers I–IV**, we argue that bistatic operation with separated transmitter and receiver is a major component in designing noise radar systems. While we know the purpose of a radar system is to survey the environment for targets, we have in this thesis and in the relevant publications mostly ignored the question of an important use case for noise radar in favour of pulsed radar operation. A non-periodic waveform does not suffer from the ambiguities of a pulsed system, but instead causes self-interference through the correlation noise floor. It can be argued that a radar operating with a non-periodic waveform using a large instantaneous bandwidth is clandestine as its signals will be difficult for an adversarial electronic surveillance system to detect or identify as a radar. This may be the case, but quantitative analysis on this topic tends to be confidential. Even if the use case of a noise radar system may be called into question, the ability to process large time-bandwidth products of signals with arbitrary waveforms is nevertheless useful, with passive radar using existing transmitters of opportunity as a clear application. Further development of the clutter suppression signal processing techniques will remain important for these applications, and radar in general, for the foreseeable future.

While the experimental side of the project turned to noise radar, the theoretical side was not abandoned. Instead, we continued the theory project with a broader scope of within quantum metrology, producing **Paper VII** and **Paper VIII**. Since these papers and their results are theoretical in nature, and the tools are purely mathematical, they serve as a sharp contrast to the work with noise radar, where the theoretical analysis could be performed with access to real-world experimental data. When working with relatively abstract quantities such as quantum Fisher information, the results can sometimes be quite subtle, with many technical details and transparent assumptions needed for interpretation.

Ultimately, sensing and metrology will remain relevant and more devices may have to account for quantum effects as measurement sensitivity is improved ever further. It shall be interesting to see how the experimental methods continue to develop. When pushing against the uncertainties of quantum mechanics, a deep understanding of the limitations and possibilities is paramount. At this point in time, radars are impressively sensitive technological systems able to detect extremely faint signals in large amounts of data. However, most radars operate at microwave frequencies with finite temperatures and, in these environments and power levels, quantum effects are washed out and classical descriptions are perfectly sufficient. It would appear that, at least for now, quantum radar will remain an interesting research topic rather than a revolutionary paradigm for the field of radar as a whole.

# Appendices

Appendix A

# Statistics

The relations presented here may be found in any graduate textbook on statistics or statistical modelling, see *e.q.*, Refs. [70, 72, 74].

## A.1 Complex normal distribution

Let $\mathbf{z}$ be a complex random vector distributed according to the probability density function

$$p\left(\mathbf{z};\boldsymbol{\mu},\boldsymbol{\Sigma}\right)=\frac{\exp\left[-\left(\mathbf{x}-\boldsymbol{\mu}\right)^{\dagger}\boldsymbol{\Sigma}^{-1}\left(\mathbf{x}-\boldsymbol{\mu}\right)\right]}{\pi^{N}\det\boldsymbol{\Sigma}} \tag{A.1}$$

with mean $\boldsymbol{\mu}$ and covariance matrix $\boldsymbol{\Sigma}$. Then $z$ is distributed according to the complex normal distribution, which we denote as $\mathbf{z}\sim\mathcal{CN}\left(\boldsymbol{\mu},\boldsymbol{\Sigma}\right)$.

In the circularly symmetric case with diagonal covariance matrix, *i.e.*, $\mathbf{z}\sim\mathcal{CN}\left(\boldsymbol{\mu},\sigma^{2}\mathbb{I}\right)$, we have $\mathfrak{Re}[\mathbf{z}]\sim\mathcal{N}\left(\mathfrak{Re}(\boldsymbol{\mu}),\frac{\sigma^{2}}{2}\mathbb{I}\right)$ and $\mathfrak{Im}[\mathbf{z}]\sim\mathcal{N}\left(\mathfrak{Im}(\boldsymbol{\mu}),\frac{\sigma^{2}}{2}\mathbb{I}\right)$ with $\mathfrak{Re}[\mathbf{z}]$ independent of $\mathfrak{Im}[\mathbf{z}]$.

## A.2 Power and ratio statistics

Here, $\chi^{2}_{D}$ denotes the chi-squared distribution with $D$ degrees of freedom and $F_{d_1,d_2}$ denotes the $F$ distribution with $d_1$ and $d_2$ degrees of freedom. If $\mathbf{z}\sim\mathcal{CN}\left(\mathbf{0},\sigma_{Z}^{2}\mathbb{I}_{M}\right)$ and $\mathbf{w}\sim\mathcal{CN}\left(\mathbf{0},\sigma_{W}^{2}\mathbb{I}_{M}\right)$, then

$$\mathbb{E}|\mathbf{z}^{\dagger}\mathbf{w}|^{2}=\sigma_{Z}^{2}\sigma_{W}^{2}M. \tag{A.2}$$

If $\mathbf{z} \sim \mathcal{CN}\left(\boldsymbol{\mu}, \sigma^2 \mathbb{I}_M\right)$ and $u = \frac{2}{\sigma^2}||\mathbf{z} - \boldsymbol{\mu}||^2$. Then $u \sim \chi^2_{2M}$ with $\mathbb{E}[u] = 2M$ and $\mathrm{var}[u] = 4M$ such that

$$\begin{aligned} \mathbb{E}\left[u^2\right] &= \mathrm{var}[u] + (\mathbb{E}[u])^2 \\ &= 4M(M+1). \end{aligned} \tag{A.3}$$

If $u \sim \chi^2_P$ and $v \sim \chi^2_Q$, then $\frac{u/P}{v/Q} \sim F_{P,Q}$.

If $\mathbf{z} \sim \mathcal{CN}\left(\mathbf{0}, \sigma_Z^2 \mathbb{I}_M\right)$ and $\mathbf{w} \sim \mathcal{CN}\left(\mathbf{0}, \sigma_W^2 \mathbb{I}_N\right)$, then

$$\frac{\frac{2||\mathbf{z}||^2}{\sigma_Z^2}/2M}{\frac{2||\mathbf{w}||^2}{\sigma_W^2}/2N} = \frac{N||\mathbf{z}||^2\sigma_W^2}{M||\mathbf{w}||^2\sigma_Z^2} \sim F_{2M,2N}. \tag{A.4}$$

In particular, we have use of the distribution of the variable $s \sim F_{2,2N}$ with the probability density function

$$p_{F_{2,2N}}(s) = \left(1 + \frac{s}{N}\right)^{-N-1}. \tag{A.5}$$

Appendix B

# Linear Algebra

The relations presented here may be found in standard reference literature on linear algebra, see *e.g.*, Ref. [122].

## B.1 Matrix vectorisation

The matrix vectorisation maps a matrix of size $M \times N$ to a vector of size $MN \times 1$ by stacking the columns. That is, for the matrix

$$\mathbf{A} = \begin{bmatrix} \mathbf{a}_1 & \mathbf{a}_2 & \dots & \mathbf{a}_N \end{bmatrix}, \tag{B.1}$$

where $\mathbf{a}_n$ are column vectors, the vectorisation is

$$\operatorname{vec} \mathbf{A} = \begin{bmatrix} \mathbf{a}_1 \\ \mathbf{a}_2 \\ \vdots \\ \mathbf{a}_N \end{bmatrix}. \tag{B.2}$$

The vectorisation of a matrix product satisfies

$$\operatorname{vec}[\mathbf{ABC}] = \left[\mathbf{C}^\top \otimes \mathbf{A}\right] \operatorname{vec} \mathbf{B}, \tag{B.3}$$

which is known as *Roth's Relationship*.

## B.2 Pseudoinverse and Composite projections

Let $\mathbf{A}$ be a matrix. The Moore-Penrose pseudoinverse $\mathbf{A}^+$ of $\mathbf{A}$ is the unique matrix that satisfies

$$\begin{aligned} \mathbf{AA}^+\mathbf{A} = \mathbf{A}, \quad \mathbf{A}^+\mathbf{AA}^+ = \mathbf{A}^+, \\ \left[\mathbf{A}^+\mathbf{A}\right]^\dagger = \mathbf{A}^+\mathbf{A}, \quad \left[\mathbf{AA}^+\right]^\dagger = \mathbf{AA}^+. \end{aligned} \tag{B.4}$$

Let $\mathbf{M} = \begin{bmatrix} \mathbf{A} & \mathbf{B} \end{bmatrix}$ be an $m \times n$ matrix with $m > n$. The projection matrix onto the column space of $\mathbf{M}$ is

$$\mathbf{P}_{\mathbf{M}} = \mathbf{P}_{\check{\mathbf{A}}} + \mathbf{P}_{\mathbf{B}} = \mathbf{P}_{\mathbf{A}} + \mathbf{P}_{\check{\mathbf{B}}}, \tag{B.5}$$

where $\check{\mathbf{A}} = \mathbf{P}_{\mathbf{B}}^{\perp}\mathbf{A}$ with $\mathbf{P}_{\mathbf{B}}^{\perp} = \mathbb{I} - \mathbf{A}\mathbf{A}^{+}$, and equivalently for $\check{\mathbf{B}}$. If $\operatorname{rank}\mathbf{M} = n$, the Moore-Penrose pseudoinverse is [123]

$$\mathbf{M}^{+} = \begin{bmatrix} \check{\mathbf{A}}^{+} \\ \check{\mathbf{B}}^{+} \end{bmatrix}. \tag{B.6}$$

# Bibliography


[1] G. Galati. *100 Years of Radar*. 1st ed. Springer International Publishing Switzerland, 2016. ISBN: 978-3-319-00583-6. DOI: 10.1007/978-3-319-00584-3.

[2] D. S. Ilcev. "The development of maritime radar. Part 1: Before the Second World War". In: *International Journal of Maritime History* 32.4 (2020), pp. 996–1007. DOI: 10.1177/0843871420977963.

[3] C. W. Helstrom. "Quantum detection and estimation theory". In: *Journal of Statistical Physics* 1 (1969), pp. 231–252.

[4] S. Pirandola et al. "Advances in photonic quantum sensing". In: *Nature Photonics* 12 (2018), pp. 724–733. DOI: 10.1038/s41566-018-0301-6.

[5] J. Aasi et al. "Enhanced sensitivity of the LIGO gravitational wave detector by using squeezed states of light". In: *Nature Photonics* 7.8 (2013), pp. 613–619. DOI: 10.1038/nphoton.2013.177.

[6] L. McCuller et al. "Frequency-Dependent Squeezing for Advanced LIGO". In: *Phys. Rev. Lett.* 124 (2020), p. 171102. DOI: 10.1103/PhysRevLett.124.171102.

[7] B. M. Horton. "Noise-Modulated Distance Measuring Systems". In: *Proceedings of the IRE* 47 (1959), pp. 821–828.

[8] K. Savci et al. "Trials of a Noise-Modulated Radar Demonstrator– First Results in a Marine Environment". In: *2019 20th International Radar Symposium (IRS)*. 2019, pp. 1–9. DOI: 10.23919/IRS.2019.8768194.

[9] G. Galati et al. "Noise Radar Technology: Waveforms Design and Field Trials". In: *Sensors* 21 (2021).

[10] B. Stec and W. Susek. "Theory and Measurement of Signal-to-Noise Ratio in Continuous-Wave Noise Radar". In: *Sensors* 18 (2018). 1445, pp. 1–11. DOI: 10.3390/s18051445.

[11] G.-S. Liu et al. "Random signal radar - a winner in both the military and civilian operating environments". In: *IEEE Transactions on Aerospace and Electronic Systems* 39.2 (2003), pp. 489–498. DOI: 10.1109/TAES.2003.1207261.

[12] T. Thayaparan, M. Daković, and L. Stanković. "Mutual interference and low probability of interception capabilities of noise radar". In: *IET Radar, Sonar & Navigation* 2 (4 2008), 294–305(11). ISSN: 1751-8784. DOI: 10.1049/iet-rsn:20070146.

[13] G. Galati et al. "Counter-Interception and Counter-Exploitation Features of Noise Radar Technology". In: *Remote Sensing* 13.22 (2021). DOI: 10.3390/rs13224509.

[14] R. M. Narayanan. "Through-wall radar imaging using UWB noise waveforms". In: *Journal of the Franklin Institute* 345 (2008), pp. 659–678.

[15] W. Susek and B. Stec. "Through-the-wall detection of human activities using a noise radar with microwave quadrature correlator". In: *IEEE Transactions on Aerospace and Electronic Systems* 51.1 (2015), pp. 759–764. DOI: 10.1109/TAES.2014.130003.

[16] W. Susek, M. Knioła, and B. Stec. "Buried objects detection using noise radar". In: *2018 22nd International Microwave and Radar Conference (MIKON)*. 2018, pp. 461–463. DOI: 10.23919/MIKON.2018.8405256.

[17] K. Lukin et al. "Ka-band bistatic ground-based noise waveform SAR for short-range applications". In: *IET Radar, Sonar & Navigation* 2 (4 2008), 233–243(10). DOI: 10.1049/iet-rsn:20080017.

[18] F. Colone, R. Cardinali, and P. Lombardo. "Cancellation of clutter and multipath in passive radar using a sequential approach". In: *2006 IEEE Conference on Radar*. 2006, pp. 1–7. DOI: 10.1109/RADAR.2006.1631830.

[19] R. Cardinali et al. "Comparison of Clutter and Multipath Cancellation Techniques for Passive Radar". In: *2007 IEEE Radar Conference*. 2007, pp. 469–474. DOI: 10.1109/RADAR.2007.374262.

[20] F. Colone et al. "A multistage processing algorithm for disturbance removal and target detection in passive bistatic radar". In: *IEEE Transactions on aerospace and electronic systems* 45.2 (2009), pp. 698–722.

[21] E. H. Allen and M. Karageorgis. "Radar systems and methods using entangled quantum particles". U.S. pat. 7375802B2. L. Martin. May 2008.

[22] M. Lanzagorta. *Quantum Radar*. Springer Nature Switzerland AG 2022, 2011. ISBN: 978-3-031-02515-0. DOI: 10.1007/978-3-031-02515-0.

[23] R. G. Torromé, N. B. Bekhti-Winkel, and P. Knott. "Introduction to quantum radar". In: *arXiv:2006.14238 [quant.ph]* (2021). DOI: 10.48550/arXiv.2006.14238.

[24] G. Sorelli et al. "Detecting a Target With Quantum Entanglement". In: *IEEE Aerospace and Electronic Systems Magazine* 37.5 (2022), pp. 68–90. DOI: 10.1109/MAES.2021.3116323.

[25] S. Guha and Z. Dutton. "Systems and methods for quantum receivers for target detection using a quantum optical radar". U.S. pat. 8339581B2. R. B. T. Corp. Dec. 2012.

[26] S. Lloyd. "Enhanced Sensitivity of Photodetection via Quantum Illumination". In: *Science* 321.5895 (2008), pp. 1463–1465. DOI: 10.1126/science.1160627.

[27] M. F. Sacchi. "Optimal discrimination of quantum operations". In: *Phys. Rev. A* 71 (2005), p. 062340. DOI: 10.1103/PhysRevA.71.062340.

[28] M. F. Sacchi. "Entanglement can enhance the distinguishability of entanglement-breaking channels". In: *Phys. Rev. A* 72 (2005), p. 014305. DOI: 10.1103/PhysRevA.72.014305.

[29] J. H. Shapiro and S. Lloyd. "Quantum illumination versus coherent-state target detection". In: *New Journal of Physics* 11.6 (2009), p. 063045.

[30] S.-H. Tan et al. "Quantum Illumination with Gaussian States". In: *Phys. Rev. Lett.* 101 (2008), p. 253601. DOI: 10.1103/PhysRevLett.101.253601.

[31] L. Maccone and C. Ren. "Quantum Radar". In: *Phys. Rev. Lett.* 124 (2020), p. 200503. DOI: 10.1103/PhysRevLett.124.200503.

[32] S. Guha and B. I. Erkmen. "Gaussian-state quantum-illumination receivers for target detection". In: *Phys. Rev. A* 80 (2009), p. 052310. DOI: 10.1103/PhysRevA.80.052310.

[33] Q. Zhuang, Z. Zhang, and J. H. Shapiro. "Optimum Mixed-State Discrimination for Noisy Entanglement-Enhanced Sensing". In: *Phys. Rev. Lett.* 118 (2017), p. 040801. DOI: 10.1103/PhysRevLett.118.040801.

[34] R. Nair. "Discriminating quantum-optical beam-splitter channels with number-diagonal signal states: Applications to quantum reading and target detection". In: *Phys. Rev. A* 84 (2011), p. 032312. DOI: 10.1103/PhysRevA.84.032312.

[35] S. Barzanjeh et al. "Microwave Quantum Illumination". In: *Phys. Rev. Lett.* 114 (2015), p. 080503. DOI: 10.1103/PhysRevLett.114.080503.

[36] J. Hewitt. *Quantum radar can detect what's invisible to regular radar*. 2015. URL: https://www.extremetech.com/extreme/200161-quantum-radar-can-detect-whats-invisible-to-regular-radar (Accessed Dec. 10, 2022).

[37] J. Lin and P. Singer. *China Says It Has Quantum Radar: What Does That Mean?* 2016. URL: https://www.popsci.com/china-says-it-has-quantum-radar-what-does-that-mean/ (Accessed Dec. 10, 2022).

[38] E. D. Lopaeva et al. "Experimental Realization of Quantum Illumination". In: *Phys. Rev. Lett.* 110 (2013), p. 153603. DOI: 10.1103/PhysRevLett.110.153603.

[39] J. H. Shapiro. "The Quantum Illumination Story". In: *IEEE Aerospace and Electronic Systems Magazine* 35.4 (2020), pp. 8–20. DOI: 10.1109/MAES.2019.2957870.

[40] Z. Zhang et al. "Entanglement-Enhanced Sensing in a Lossy and Noisy Environment". In: *Phys. Rev. Lett.* 114 (2015), p. 110506. DOI: 10.1103/PhysRevLett.114.110506.

[41] D. G. England, B. Balaji, and B. J. Sussman. "Quantum-enhanced standoff detection using correlated photon pairs". In: *Phys. Rev. A* 99 (2019), p. 023828. DOI: 10.1103/PhysRevA.99.023828.

[42] P. S. Blakey et al. "Quantum and non-local effects offer over 40 dB noise resilience advantage towards quantum lidar". In: *Nature Communications* 13 (2022), p. 5633. DOI: 10.1038/s41467-022-33376-9.

[43] C. W. S. Chang et al. "Quantum-enhanced noise radar". In: *Applied Physics Letters* 114.11 (2019), p. 112601. DOI: 10.1063/1.5085002.

[44] D. Luong et al. "Receiver Operating Characteristics for a Prototype Quantum Two-Mode Squeezing Radar". In: *IEEE Transactions on Aerospace and Electronic Systems* 56.3 (2020), pp. 2041–2060. DOI: 10.1109/TAES.2019.2951213.

[45] S. Barzanjeh et al. "Microwave quantum illumination using a digital receiver". In: *Science Advances* 6.19 (2020). DOI: 10.1126/sciadv.abb0451.

[46] E. T. from the arXiv. *Quantum radar has been demonstrated for the first time*. 2019. URL: https://www.technologyreview.com/2019/08/23/75512/quantum-radar-has-been-demonstrated-for-the-first-time/ (Accessed Mar. 23, 2023).

[47] R. Assouly et al. "Quantum advantage in microwave quantum radar". In: *Nature Physics* 19 (2023), pp. 1418–1422. DOI: 10.1038/s41567-023-02113-4.

[48] H. Khalifa et al. "Microwave Gaussian Quantum Sensing With a CNOT Gate Receiver". In: *IEEE Access* 11 (2023), pp. 103986–103999. DOI: 10.1109/ACCESS.2023.3318484.

[49] S. Jeon et al. *Microwave Quantum Illumination with Optical Memory and Single-Mode Phase-Conjugate Receiver*. 2024. DOI: 10.48550/arXiv.2405.14118. arXiv: 2405.14118 [quant-ph].

[50] J. Angeletti et al. "Microwave quantum illumination with correlation-to-displacement conversion". In: *arXiv:2303.18206 [quant-ph]* (2023). DOI: 10.48550/arXiv.2303.18206.

[51] H. Shi, B. Zhang, and Q. Zhuang. "Fulfilling entanglement's optimal advantage via converting correlation to coherence". In: *arXiv: 2207.06609 [quant-ph]* (2022). DOI: 10.48550/arXiv.2207.06609.

[52] M. Reichert et al. "Quantum Illumination with a Hetero-Homodyne Receiver and Sequential Detection". In: *arXiv:2303.18207 [quant-ph]* (2023). DOI: 10.48550/arXiv.2303.18207.

[53] W. Khan et al. "Efficient and continuous microwave photoconversion in hybrid cavity-semiconductor nanowire double quantum dot diodes". In: *Nature Communications* 12 (2021). DOI: 10.1038/s41467-021-25446-1.

[54] K. Petrovnin et al. "Microwave Photon Detection at Parametric Criticality". In: *PRX Quantum* 5 (2 2024), p. 020342. DOI: 10.1103/PRXQuantum.5.020342.

[55] K. Durak, N. Jam, and Ç. Dindar. "Object tracking and identification by quantum radar". In: *Quantum Technologies and Quantum Information Science V*. Ed. by M. T. Gruneisen et al. Vol. 11167. International Society for Optics and Photonics. SPIE, 2019. DOI: 10.1117/12.2550479.

[56] Q. Zhuang and J. H. Shapiro. "Ultimate Accuracy Limit of Quantum Pulse-Compression Ranging". In: *Phys. Rev. Lett.* 128 (2022), p. 010501. DOI: 10.1103/PhysRevLett.128.010501.

[57] M. Reichert et al. "Quantum-enhanced Doppler lidar". In: *npj Quantum Information* 8 (2022). DOI: 10.1038/s41534-022-00662-9.

[58] U. Las Heras et al. "Quantum illumination reveals phase-shift inducing cloaking". In: *Scientific Reports* 7 (2017). DOI: 10.1038/s41598-017-08505-w.

[59] Q. Zhuang, Z. Zhang, and J. H. Shapiro. "Quantum illumination for enhanced detection of Rayleigh-fading targets". In: *Phys. Rev. A* 96 (2017), p. 020302. DOI: 10.1103/PhysRevA.96.020302.

[60] E. Jung and D. Park. "Quantum illumination with three-mode Gaussian state". In: *Quantum Information Processing* 21 (2022), p. 71. DOI: 10.1007/s11128-021-03359-8.

[61] G. Pavan and G. Galati. "Range Limitations in Microwave Quantum Radar". In: *Remote Sensing* 16.14 (2024). DOI: 10.3390/rs16142543.

[62] A. Karsa et al. "Quantum illumination and quantum radar: a brief overview". In: *Reports on Progress in Physics* 87.9 (2024), p. 094001. DOI: 10.1088/1361-6633/ad6279.

[63] L. V. Blake. *Radar range-performance analysis*. LexingtonBooks, 1980.

[64] M. I. Skolnik. *Radar handbook*. 2nd ed. McGraw-Hill, 1990.

[65] E. Kelly and R. Wishner. "Matched-filter theory for high-velocity, accelerating targets". In: *IEEE Transactions on Military Electronics* 9.1 (1965), pp. 56–69.

[66] L. Ziomek. "Comments on the generalized ambiguity function". In: *IEEE Transactions on Acoustics, Speech, and Signal Processing* 30.1 (1982), pp. 117–119.

[67] T. Ding et al. "A Novel Iterative Inner-Pulse Integration Target Detection Method for Bistatic Radar". In: *IEEE Transactions on Geoscience and Remote Sensing* 60 (2022), pp. 1–15.

[68] K. S. Kulpa and J. Misiurewicz. "Stretch Processing for Long Integration Time Passive Covert Radar". In: *2006 CIE International Conference on Radar*. Shanghai, China, 2006, pp. 1–4. DOI: 10.1109/ICR.2006.343481.

[69] K. Kulpa and Z. Czekała. "Masking effect and its removal in PCL radar". In: *IEE Proceedings - Radar, Sonar and Navigation* 152 (3 2005), 174–178(4). DOI: 10.1049/ip-rsn:20045026.

[70] S. M. Kay. *Fundamentals of Statistical Signal Processing: Volume II Detection Theory*. Prentice-Hall, Inc., 1998. ISBN: 0-13-504135-X.

[71] S. S. Wilks. "The Large-Sample Distribution of the Likelihood Ratio for Testing Composite Hypotheses". In: *The Annals of Mathematical Statistics* 9.1 (1938), pp. 60–62. ISSN: 00034851. URL: http://www.jstor.org/stable/2957648 (Accessed Apr. 3, 2023).

[72] S. M. Kay. *Fundamentals of Statistical Signal Processing: Estimation Theory*. Prentice-Hall, Inc., 1993. ISBN: 0-13-345711-7.

[73] L. L. Scharf and B. Friedlander. "Matched Subspace Detectors". In: *IEEE Transactions on signal processing* 42.8 (Aug. 1994). DOI: 10.1109/ACSSC.1993.342610.

[74] K. Siegrist. *Probability, Mathematical Statistics, and Stochastic Processes.* LibreText, 2024. URL: https://stats.libretexts.org/Bookshelves/Probability_Theory/Probability_Mathematical_Statistics_and_Stochastic_Processes_(Siegrist) (Accessed Aug. 29, 2024).

[75] A. Nelander. "Inverse Filtering for Noise Radar Processing". In: *2006 International Radar Symposium.* 2006, pp. 1–4. DOI: 10.1109/IRS.2006.4338087.

[76] K. Kulpa. *Signal processing in noise waveform radar.* Artech House, 2013.

[77] J. S. Kulpa. "Noise radar sidelobe suppression algorithm using mismatched filter approach". In: *International Journal of Microwave and Wireless Technologies* 8.6 (2016), pp. 865–869. DOI: 10.1017/S1759078716000945.

[78] F. De Palo and G. Galati. "Range sidelobes attenuation of pseudorandom waveforms for civil radars". In: *2017 European Radar Conference (EURAD).* 2017, pp. 114–117. DOI: 10.23919/EURAD.2017.8249160.

[79] J. Högbom. "Aperture synthesis with a non-regular distribution of interferometer baselines". In: *Astronomy and Astrophysics Supplement* 15 (1974), p. 417.

[80] J. Tropp. "Greed is good: algorithmic results for sparse approximation". In: *IEEE Transactions on Information Theory* 50.10 (2004), pp. 2231–2242. DOI: 10.1109/TIT.2004.834793.

[81] Y. Pati, R. Rezaiifar, and P. Krishnaprasad. "Orthogonal matching pursuit: recursive function approximation with applications to wavelet decomposition". In: *Proceedings of 27th Asilomar Conference on Signals, Systems and Computers.* Vol. 1. 1993, pp. 40–44. DOI: 10.1109/ACSSC.1993.342465.

[82] H. Zhu, W. Chen, and Y. Wu. "Efficient Implementations for Orthogonal Matching Pursuit". In: *Electronics* 9 (2020). ISSN: 2079-9292. DOI: 10.3390/electronics9091507.

[83] F. Colone et al. "Sliding extensive cancellation algorithm for disturbance removal in passive radar". In: *IEEE Transactions on Aerospace and Electronic Systems* 52.3 (2016), pp. 1309–1326. DOI: 10.1109/TAES.2016.150477.

[84] M. H. Hayes. *Statistical digital signal processing and modeling.* John Wiley & Sons, 1996.

[85] V. Ingle, S. Kogon, and D. Manolakis. *Statisical and adaptive signal processing.* Artech, 2005.

[86] M. Zatman. "How Narrow is Narrowband?" In: *IEE Proceedings-Radar, Sonar and Navigation* 145.2 (1998), pp. 85–91.

[87] R. Loudon. *The Quantum Theory of Light.* 3rd ed. Oxford University Press, 2000. ISBN: 978-0-19-850176-3.

[88] S. Barnett and P. Radmore. *Methods in Theoretical Quantum Optics.* 1st ed. Oxford University Press, 1997. ISBN: 0-19-856362-0.

[89] C. Cohen-Tannoudji, J. Dupont-Roc, and G. Grynberg. *Photons and Atoms. Introduction to Quantum Electrodynamics*. 1st ed. John Wiley & Sons, Inc., 1989. ISBN: 0-471-18433-0.

[90] H. Goldstein, C. Poole, and J. Safko. *Classical Mechanics*. 3rd ed. Pearson Education Limited, 2002. ISBN: 978-1-292-02655-8.

[91] C. Weedbrook et al. "Gaussian quantum information". In: *Rev. Mod. Phys.* 84 (2012), pp. 621–669. DOI: 10.1103/RevModPhys.84.621.

[92] G. Adesso, S. Ragy, and A. R. Lee. "Continuous variable quantum information: Gaussian states and beyond". In: *Open Systems and Information Dynamics* 21.1 & 2 (2014), p. 1440001. DOI: 10.1142/S1230161214400010.

[93] A. Serafini. *Quantum continuous variables: a primer of theoretical methods*. 1st ed. CRC press, 2017. ISBN: 978-1-4822-4634-6.

[94] M. S. Kim, F. A. M. de Oliveira, and P. L. Knight. "Properties of squeezed number states and squeezed thermal states". In: *Phys. Rev. A.* 40 (1989), pp. 2494–2503. DOI: 10.1103/PhysRevA.40.2494.

[95] G. Lindblad. "On the generators of quantum dynamical semigroups". In: *Commun.Math. Phys.* 48 (1976), pp. 119–130.

[96] V. Gorini, A. Kossakowski, and E. C. G. Sudarshan. "Completely positive dynamical semigroups of N-level systems". In: *J. Math. Phys.* 17 (1976), pp. 821–825.

[97] A. Monras and M. G. A. Paris. "Optimal Quantum Estimation of Loss in Bosonic Channels". In: *Phys. Rev. Lett.* 98 (2007), p. 160401. DOI: 10.1103/PhysRevLett.98.160401.

[98] A. Monras and F. Illuminati. "Measurement of damping and temperature: Precision bounds in Gaussian dissipative channels". In: *Phys. Rev. A* 83 (2011), p. 012315. DOI: 10.1103/PhysRevA.83.012315.

[99] R. Nair. "Quantum-Limited Loss Sensing: Multiparameter Estimation and Bures Distance between Loss Channels". In: *Phys. Rev. Lett.* 121 (2018), p. 230801. DOI: 10.1103/PhysRevLett.121.230801.

[100] J. H. Shapiro. "The Quantum Theory of Optical Communications". In: *IEEE Journal of Selected Topics in Quantum Electronics* 15.6 (2009), pp. 1547–1569. DOI: 10.1109/JSTQE.2009.2024959.

[101] S. H. Tan. "Quantum state discrimination with bosonic channels and Gaussian states". Massachusetts Institute of Technology. PhD thesis. Massachusetts Institute of Technology, 2010. URL: http://hdl.handle.net/1721.1/79253 (Accessed Nov. 12, 2022).

[102] C. M. Caves. "Quantum limits on noise in linear amplifiers". In: *Physical Review D* 26.8 (1982), pp. 1817–1839. DOI: 10.1103/PhysRevD.26.1817.

[103] D. Braun et al. "Quantum-enhanced measurements without entanglement". In: *Rev. Mod. Phys.* 90 (2018), p. 035006. DOI: 10.1103/RevModPhys.90.035006.

[104] K. M. R. Audenaert et al. "Discriminating States: The Quantum Chernoff Bound". In: *Phys. Rev. Lett.* 98 (2007), p. 160501. DOI: 10.1103/PhysRevLett.98.160501.

[105] S. Pirandola and S. Lloyd. "Computable bounds for the discrimination of Gaussian states". In: *Phys. Rev. A* 78 (2008), p. 012331. DOI: 10.1103/PhysRevA.78.012331.

[106] T. Kailath. "The Divergence and Bhattacharyya Distance Measures in Signal Selection". In: *IEEE Transactions on Communication Technology* 15.1 (1967), pp. 52–60. DOI: 10.1109/TCOM.1967.1089532.

[107] R. Nair and M. Gu. "Fundamental limits of quantum illumination". In: *Optica* 7.7 (2020), pp. 771–774. DOI: 10.1364/OPTICA.391335.

[108] J. Calsamiglia et al. "Local discrimination of mixed states". In: *Physical review letters* 105.8 (2010), p. 080504. DOI: 10.1103/PhysRevLett.105.080504.

[109] A. Karsa and S. Pirandola. "Classical benchmarking for microwave quantum illumination". In: *IET Quantum Communication* 2.4 (2021), pp. 246–257. DOI: 10.1049/qtc2.12025.

[110] M. M. Wilde et al. "Gaussian Hypothesis Testing and Quantum Illumination". In: *Phys. Rev. Lett.* 119 (2017), p. 120501. DOI: 10.1103/PhysRevLett.119.120501.

[111] Q. Zhuang, Z. Zhang, and J. H. Shapiro. "Entanglement-enhanced Neyman-Pearson target detection using quantum illumination". In: *J. Opt. Soc. Am. B* 34 (2017), pp. 1567–1572. DOI: 10.1364/JOSAB.34.001567.

[112] F. Hiai and D. Petz. "The proper formula for relative entropy and its asymptotics in quantum probability". In: *Communications in mathematical physics* 143 (1991), pp. 99–114. DOI: 10.1007/BF02100287.

[113] T. Ogawa and H. Nagaoka. "Strong converse and Stein's lemma in quantum hypothesis testing". In: *IEEE Transactions on Information Theory* 46.7 (2000), pp. 2428–2433. DOI: 10.1109/18.887855.

[114] G. De Palma and J. Borregaard. "Minimum error probability of quantum illumination". In: *Phys. Rev. A* 98 (2018), p. 012101. DOI: 10.1103/PhysRevA.98.012101.

[115] K. Li. "Second-order asymptotics for quantum hypothesis testing". In: *The Annals of Statistics* 42.1 (2014), pp. 171–189. DOI: 10.1214/13-AOS1185.

[116] Z. Gong et al. "Fundamental Limits of Loss Sensing over Bosonic Channels". In: *2021 IEEE International Symposium on Information Theory (ISIT)*. 2021, pp. 1182–1187. DOI: 10.1109/ISIT45174.2021.9517810.

[117] Z. Gong et al. "Quantum-Enhanced Transmittance Sensing". In: *IEEE Journal of Selected Topics in Signal Processing* (2022), pp. 1–17. DOI: 10.1109/JSTSP.2022.3222680.

[118] C. Sánchez Muñoz, G. Frascella, and F. Schlawin. "Quantum metrology of two-photon absorption". In: *Phys. Rev. Res.* 3 (2021). DOI: 10.1103/PhysRevResearch.3.033250.

[119] S. Panahiyan et al. "Two-photon-absorption measurements in the presence of single-photon losses". In: *Phys. Rev. A* 106 (2022). DOI: 10.1103/PhysRevA.106.043706.

[120] S. Panahiyan et al. "Nonlinear interferometry for quantum-enhanced measurements of multiphoton absorption". In: *Phys. Rev. Lett.* 130 (2023). DOI: 10.1103/PhysRevLett.130.203604.

[121] G. Galati and G. Pavan. *On Target Detection by Quantum Radar (Preprint)*. 2024. DOI: 10.48550/arXiv.2403.00047. arXiv: 2403.00047 [quant-ph].

[122] K. B. Petersen and M. S. Pedersen. *The Matrix Cookbook*. Version 20121115. 2012. URL: http://www2.compute.dtu.dk/pubdb/pubs/3274-full.html (Accessed July 1, 2024).

[123] J. K. Baksalary and O. M. Baksalary. "Particular formulae for the Moore-Penrose inverse of a columnwise partitioned matrix". In: *Linear Algebra and its Applications* 421 (2007), pp. 16–23. DOI: 10.1016/j.laa.2006.03.031.